Continental collision, orogenesis and arc magmatism of the Miocene Maramuni arc, Papua New Guinea

Robert J. Holm, Carl Spandler, Simon W. Richards

PII: S1342-937X(14)00286-X
DOI: doi: 10.1016/j.gr.2014.09.011
Reference: GR 1331

To appear in: *Gondwana Research*

Received date: 27 March 2014
Revised date: 3 September 2014
Accepted date: 6 September 2014

Please cite this article as: Holm, Robert J., Spandler, Carl, Richards, Simon W., Continental collision, orogenesis and arc magmatism of the Miocene Maramuni arc, Papua New Guinea, *Gondwana Research* (2014), doi: 10.1016/j.gr.2014.09.011

Continental collision, orogenesis and arc magmatism of the Miocene Maramuni arc, Papua New Guinea.

Robert J. Holm*, Carl Spandler, Simon W. Richards

College of Science, Technology and Engineering,

James Cook University, Douglas, Townsville, Queensland 4811, Australia

*corresponding author: *rob.holm@my.jcu.edu.au*

ABSTRACT

The Maramuni arc represents the only continuous record of the tectonic evolution of Papua New Guinea during the Miocene, and hence provides an opportunity to gain insight into subduction dynamics, orogenesis and crustal processes that operated throughout this dynamic period. We present an integrated U-Pb geochronology, Hf isotope and geochemical investigation of the Maramuni arc utilizing a suite of intrusive rocks from the Kainantu region of the eastern Papuan Highlands that span the Late Miocene from ca. 12 Ma to 6 Ma. The magmatic rocks formed from ca. 12–9 Ma have compositional affinities of subduction-zone magmas, but record increasing incompatible trace element contents and decreasing εHf with time, which we interpret to reflect a progressive increase in the crustal component of the magmas. Porphyry suites emplaced at 7.5-6 Ma are distinct from the older magmatic rocks by their marked HREE-depletion, which reflects a dramatic shift in arc-mantle dynamics. Based on these results we propose a revised geodynamic model for the tectonic

evolution of Papua New Guinea involving arrival of the Australian continent at a north-dipping Pocklingon trough from ca. 12 Ma. Continent collision then led to growth of the New Guinea Orogen from 12 Ma aided by underthrusting of the leading continental margin, which contributed crustal material to magma-genesis at ca. 9 Ma. From ca. 7 Ma slab break-off and lithospheric delamination are reflected in a second phase of orogenesis that produced the HREE-depleted geochemical signatures of the contemporaneous magmatic rocks.

Keywords: Papua New Guinea; arc magmatism; continental collision; geochemisty; Hf isotopes

1. INTRODUCTION

Cenozoic tectonics of the southwest Pacific are defined by multiple episodes of large-scale tectonic reorganization driven primarily by major collision events, such as the collision of the Ontong Java Plateau with the Melanesian arc (Petterson et al., 1999; Hall, 2002; Mann and Taira, 2004; Holm et al., 2013), and collision of the Australian continent with New Guinea (Cloos et al., 2005; Hill and Hall, 2003; Schellart et al., 2006; Whattam, 2009). However, the nature and timing of these events is under dispute, which in turn compromises our understanding of even the basic regional geodynamic framework of the southwest Pacific. Papua New Guinea is critical to our understanding of southwest Pacific tectonics as it lies within a zone of oblique convergence between the Ontong Java Plateau of the Pacific plate, and the Australian continent (Fig. 1), and records a complex tectonic history of terrane collision and orogenesis, arc magmatism, microplate development and varying subduction

dynamics. Of additional significance, the Maramuni arc of Papua New Guinea and West Papua hosts some of the world's largest subduction-related porphyry ore deposits including Ok Tedi, Frieda River, Porgera and Grasberg (e.g. Hill et al., 2002; Sillitoe, 2010).

Much of the tectonic framework of Papua New Guinea remains the subject of debate due to uncertainty over the timing and nature of tectonic events and plate boundaries in the region. Consequently, an array of contrasting tectonic reconstructions for the region have been proposed (e.g. Abbott, 1995; Hill and Raza, 1999; Hall, 2002; Hill and Hall, 2003; Cloos et al., 2005; Schellart et al., 2006; Whattam et al., 2008; Whattam, 2009; Davies, 2012). Improving our understanding of Papua New Guinea tectonics requires a comprehensive and quantitative dataset for the timing and nature of geodynamics within the region. The Maramuni arc of Papua New Guinea represents the only continuous tectonic element throughout the dynamic Miocene, marked by complex collision events and orogenesis. Therefore, the Maramuni arc presents an ideal setting to examine the tectonic and geodynamic processes associated with arc magmatism, subduction, orogenesis, continental growth and mineralization.

Studies of the nature of arc magmatism through time - particularly during periods of tectonic change - can provide us with insights into subduction dynamics and crustal processes that may be difficult to resolve via other means. In this paper we present a detailed geochemical and geochronological investigation into the Middle–Late Miocene evolution of Papua New Guinea using the Maramuni arc as a record for the dynamic tectonic processes during this time. We present new datasets of zircon U-Pb geochronology and Hf isotopes, as well as detailed geochemistry of igneous rocks of

the Maramuni arc from the porphyry mineralization prospects of Wamum and Kokofimpa of the Kainantu region in the eastern Papuan Highlands (Fig. 1). Considering these new data together with previous data and tectonic models of Papua New Guinea, we propose a revised geodynamic model to help explain the complex tectonic history of the region.

2. GEOLOGICAL SETTING AND SAMPLES

2.1 Tectonic Setting

The island of New Guinea, incorporating Papua New Guinea and West Papua, Indonesia, is composed of terranes accreted to the northern Australian continental margin during the Cenozoic (Hill and Hall 2003; Crowhurst et al., 2004; Davies, 2012). Current knowledge of Papua New Guinea geology and tectonics is covered in depth by the recent review articles of Baldwin et al. (2012) and Davies (2012). The focal point of New Guinea geology is the New Guinea Orogen or Central Range, which runs along the east-west axis of the island and comprises the Papuan Fold and Thrust Belt and uplifted areas of the New Guinea Mobile Belt (Fig. 1). The Papuan Fold and Thrust Belt is an accretionary orogen of sedimentary cover rocks developed on Australian continental basement (Hill and Gleadow, 1989; Craig and Warvakai, 2009) and buttressed against variably deformed sedimentary, metamorphic and crystalline rocks of the New Guinea Mobile Belt (Hill and Raza, 1999; Davies, 2012). The Lagaip and Bundi fault zones mark the contact zone between the two orogenic belts and comprise uplifted and exhumed Australian continental basement rocks at the rear of the Papuan Fold and Thrust Belt. Growth of the New Guinea Orogen is

generally accepted to have occurred in two distinct phases of uplift and deformation, with initial uplift from 12 Ma (Hill and Raza, 1999; Cloos et al., 2005) and a secondary event from approximately 6 Ma that contributed largely to the development of the Papuan Fold and Thrust Belt (Hill and Gleadow, 1989; Hill and Raza, 1999; Cloos et al., 2005).

The Late Cenozoic Maramuni arc intrudes the New Guinea Orogen (Fig. 1). The earliest igneous rocks were emplaced into the New Guinea Mobile Belt in the Late Oligocene and were coincident with initiation of subduction beneath New Guinea (Davies et al., 1987; Lock et al., 1987; Hill and Raza, 1999; Cloos et al., 2005). Evidence for the nature of this early arc activity, however, is sparsely exposed at the surface. In the north of Papua New Guinea the early Maramuni arc is buried beneath the Sepik-Ramu sedimentary basins associated with Late Oligocene collision of the North Sepik arc terranes (Fig. 1; Crowhurst et al., 1996; Davies, 2012), and in northeast Papua New Guinea by underthrusting of the leading arc rocks and continental margin beneath the Adelbert and Finisterre Terranes during Plio-Pleistocene arc-continent collision (Abbott et al., 1994; Woodhead et al., 2010; Holm and Richards, 2013).

During the Late Miocene magmatism migrated south into the Papuan Fold and Thrust Belt (Page, 1976; Rogerson and Williamson, 1985; Davies, 1990), while recent Pliocene and Quaternary igneous activity is almost exclusively hosted within the Papuan Fold and Thrust Belt and stable Australian continental crust of the Fly Platform (Fig. 1). It is worth noting that the source of Pliocene and Quaternary magmatism has not yet been conclusively determined; it has been attributed to partial

melting of the upper mantle following arc-continent collision and crustal thickening (Johnson et al., 1978; Johnson and Jaques, 1980), or alternatively, to lithospheric delamination and adiabatic decompression of the mantle following arc-continent collision (Cloos et al., 2005). Although the relationship between Pliocene and Quaternary magmatism with earlier arc activity is not yet conclusively established, we define the Maramuni arc as comprising all Late Cenozoic magmatism with a subduction-related geochemical signature.

There are two leading but contrasting hypotheses regarding the tectonic setting for emplacement of the Maramuni arc and the associated subduction geometry during this period. Much of the difficulty in establishing the subduction orientation arises from the absence of a seismically active subducted slab in the mantle at the present day (Hall and Spakman, 2002). The generally accepted view invokes south-dipping subduction at the Trobriand trough to the north of New Guinea (e.g. Hamilton, 1979; Ripper, 1982; Davies et al., 1984; Davies et al., 1987; Lock et al., 1987; Davies, 2012). This idea was founded on the premise of a "trench-like feature" that is spatially associated with Late Cenozoic magmatism of the Maramuni arc (Johnson et al., 1978; Hamilton, 1979). Although little subsequent work has tested this hypothesis, the model has been accepted in recent literature (e.g. Hall, 2002; Cloos et al., 2005; Schellart et al., 2006; Davies, 2012; Smith, 2013). Collision of the Ontong Java Plateau with the Melanesian arc in the Early Miocene is often invoked as initiating south–dipping subduction at the Trobriand trough (Petterson et al., 1999; Hall, 2002; Hill and Hall, 2003; Schellart et al., 2006). Subsequent arc-continent collision at the Trobriand trough is often attributed to the development of the New Guinea Orogen from approximately 12 Ma (Davies, 1990; Abbott et al., 1994; Hill and Raza, 1999).

The alternate hypothesis appeals to a north-dipping subduction system located to the south of New Guinea (e.g. Hill and Hall, 2003; Cloos et al., 2005). Cloos et al. (2005) propose northwards subduction to the south of West Papua but at the same time retains reference to southwards subduction at the Trobriand trough in Papua New Guinea creating inconsistencies between the tectonic evolution of West Papua and Papua New Guinea. This northwards subduction associated with West Papua is said to be responsible for convergence between the leading northern Australian continental margin and an outer arc terrane, in addition to magmatism of the Maramuni arc. Cloos et al. (2005) also proposed that arrival and collision of the Australian continent with the outboard terrane is responsible for growth of the New Guinea Orogen from 12 Ma. The proposed north-dipping subduction zone has also been invoked by other authors as a zone of earlier Cenozoic convergence between the Australian continent and an outboard terrane (e.g. Pigram and Symonds, 1991; Schellart et al., 2006; Davies, 2012).

2.2 Regional Geology

The Kainantu region is situated in the eastern New Guinea Orogen (Fig. 1). The area is bounded to the northeast by the recently accreted Finisterre Terrane, and to the east and southeast by the Aure trough. Basement rocks in the region outcrop as the Upper Permian–Lower Triassic Goroka Formation and Middle–Upper Triassic Bena Bena Formation (Fig. 1c; Espi et al., 2007; Van Wyck and Williams, 2002). Both the Goroka and Bena Bena Formations comprise sedimentary rocks that were regionally metamorphosed to greenschist facies in the early Mesozoic (Tingey and Grainger,

1976; Van Wyck and Williams, 2002). The Bena Bena Formation is unconformably overlain by the Upper Oligocene–Early Miocene Omaura Formation, which in turn is conformably overlain by sedimentary, volcanoclastic and volcanic rocks of the Lower–Middle Miocene Yaveufa Formation. Regional uplift associated with growth of the New Guinea Orogen in the Late Miocene–Pliocene led to deposition of Pliocene–Quaternary sediments that fill the Ramu-Markham valley and areas of low relief (Tingey and Grainger, 1976). Igneous activity in the region is generally classified as belonging to either the Lower–Middle Miocene Akuna intrusive complex or the Middle–Upper Miocene Bismarck and Elandora intrusive complexes that are exposed as eroded volcano-plutonic centers (Corbett et al., 1994; Espi et al., 2007; Page, 1976; Rogerson and Williamson, 1985).

The Wamum Cu-Au porphyry prospect is situated adjacent to the Aure trough at the eastern margin of the New Guinea Orogen (Fig. 1). Host rocks for the prospect comprise thickly bedded andesitic volcanics of the Lower to Middle Miocene Yaveufa Formation, that are locally underlain by a conglomerate sequence of uncertain relationship to the volcanics (Shedden, 1990). Mineralization at Wamum is centred on small stocks of tonalite porphyry intruded into the andesitic volcanic sequences. Hydrothermal alteration at Wamum is extensive and is typified by moderate potassic and propylitic alteration in the andesites, and propylitic and weak potassic alteration in the tonalite porphyry. Primary pyrite and chalcopyrite mineralization at Wamum dominantly occurs as a fracture-controlled network in the tonalite porphyry (Shedden, 1990).

The Kokofimpa Cu-Au porphyry prospect is located near Bilimoia, some 14 km northeast of Kainantu (Fig. 1). Basement rocks of the Bena Bena Formation are exposed in the district and these are intruded by several intrusive phases that Corbett et al. (1994) classified as belonging to the Akuna and Elandora intrusive complexes. The source of porphyry mineralization at Kokofimpa is inconclusive and has been attributed to different intrusions, either granodiorites of Akuna association (Corbett et al., 1994) or a diorite porphyry (Tosdal, 2009), and hosted within granitoids of the Akuna complex (Corbett et al., 1994). The alteration system comprises of potassic, sericitic, argillic and advanced argillic alteration and the mineralization consists of chalcopyrite, bornite and pyrite, with molybdenite occuring locally in late veins (Corbett et al., 1994; Tosdal, 2009).

2.3 Samples

Rock samples were obtained in conjunction with Barrick Australia from the Wamum and Kokofimpa porphyry prospects of the Kainantu region. Rock material was sampled from diamond drill core from Wamum and Kokofimpa to include a representative sample of each logged rock unit. These sampling intervals were further scrutinized to minimize abundance of veining and effects of alteration in an effort to reflect compositions most similar to the unaltered rock. One additional field sample was collected from outcrop in Kora Creek, adjacent to the Kokofimpa prospect. Given the pervasive nature of alteration in porphyry mineral systems, rock classifications are inferred from preserved minerals and textures. Table 1 provides the location and description of the rock types sampled; photomicrographs of representative samples are included in the supplementary material.

We divide the sample set into three categories: the Wamum prospect porphyritic tonalite samples, Kokofimpa prospect porphyritic tonalite samples, and Kokofimpa prospect porphyritic dacite samples. The Wamum prospect suite comprises two samples, BWDD4 482 and 585; both are foliated plagioclase (andesine composition) porphyries with preferentially aligned zoned plagioclase phenocryts that make up approximately 50% of the rock mass in fresh samples. These phenocrysts are set within a matrix comprised primarily of quartz, biotite and magnetite. Tonalites of the Kokofimpa prospect (BKDD22 468, 472, 475, 511, 560, and 658) exhibit a porphyritic texture comprising plagioclase phenocrysts with a matrix consisting of medium–coarse grains of quartz, plagioclase, biotite and magnetite. Samples BKDD22 511, 560 and 658 also feature abundant disseminated pyrite and chalcopyrite. Porphyritic dacites of the Kokofimpa prospect can be divided into two varieties. BKDD22 546 is a plagioclase-quartz-biotite porphyry and an associated matrix of quartz, plagioclase and magnetite. BKDD22 582 and KKS01 are similar in nature to the BKDD22 546 porphyry but have distinct highly-fractured plagioclase phenocrysts.

Overprinting alteration is common in most samples from the Kokofimpa prospect with a greater apparent intensity of alteration within the tonalite sample suite. Samples from the Wamum prospect are only weakly altered. Seritization is the dominant alteration type in all samples, and is often coupled with chloritization. Plagioclase is commonly completely replaced by sericite, however, some samples exhibit only partial alteration of plagioclase, dominantly through fractures in the

crystals. This style of alteration is typical of sericitic or chlorite-sericite alteration in porphyry complexes (Sillitoe, 2010).

3. METHODS

Samples with minimal evidence of alteration were selected for geochemical analysis. Weathering rinds were removed from surface samples with a hydraulic splitter. The cored surfaces of the drill core samples were ground off with diamond implanted grinders and subsequently washed in an ultrasonic bath to minimize contamination from drilling. Rock material was then milled to a fine powder in a tungsten carbide ring mill at James Cook University (JCU), Townsville, Australia. Major and trace element analyses were analyzed at the Advanced Analytical Centre, JCU by conventional X-ray fluorescence (XRF) and ICP-MS methods using the same techniques and set-up outlined in Holm et al. (2013). NIST SRM 610 glass was used as a bracketed external standard for LA-ICP-MS analyses using the standard reference values of Spandler et al. (2011). Data were quantified using Si (as previously determined by XRF) as the internal standard, and data were processed off-line using the Glitter software (Van Achterbergh et al., 2001).

Eight samples were selected for U-Pb dating of zircons. These include two drill core samples from Wamum, five drill core samples from Kokofimpa, and one surface field sample from Kokofimpa. Mineral separation to extract zircon crystals was carried out at JCU in a standard four-step process. Samples were crushed and milled to 500 μm, washed to remove the clay proportion, and separated by a combination of heavy liquid density separation and magnetic separation. Zircon crystals were hand picked and

mounted in epoxy with grains of GJ1 (Jackson et al., 2004), Temora 2 (Black et al., 2004) and Fish Canyon Tuff zircon standards (Schmitz and Bowring, 2001; Renne et al., 2010). Epoxy mounts were polished and carbon-coated. Cathodoluminescence (CL) images of all zircon crystals were obtained using a Jeol JSM5410LV scanning electron microscope equipped with a Robinson CL detector, housed at JCU.

All U-Pb dating work was completed at the Advanced Analytical Centre, JCU. U-Pb dating of zircons was conducted by laser ablation ICP-MS using the instrumentation and methods described in Tucker et al. (2013) and Holm et al. (2013). For quantification of U and Th concentration in zircon samples, analysis of the NIST SRM 612 reference glass was conducted at the beginning, middle and end of every analytical session, with ^{29}Si used as the internal standard assuming perfect zircon stoichiometry. Zircons were analyzed with a beam spot diameter of either 60 or 44 μm and selection of analytical sample spots was guided by CL images and targeted both cores and rims. Data reduction was carried out using the Glitter software (Van Achterbergh et al., 2001). All time-resolved single isotope signals from standards and samples were filtered for signal spikes or perturbations related to inclusions and fractures. Subsequently, the most stable and representative isotopic ratios were selected taking into account possible mixing of different age domains and zoning. Drift in instrumental measurements was corrected following analysis of drift trends in the raw data using measured values for the GJ1 primary zircon standard. Analyses of Temora 2 and Fish Canyon Tuff zircons were used for verification of GJ1 following drift correction (see supplementary material). Background corrected analytical count rates, calculated isotopic ratios and 1σ uncertainties were exported for further processing and data reduction.

Initial Th/U disequilibrium during zircon crystallization is related to the exclusion of ^{230}Th due to isotope fractionation, and resulting in a deficit of measured ^{206}Pb as a ^{230}Th decay product (Schärer, 1984; Parrish, 1990). Zircon ages of <10 m.y. are particularly susceptible to this disequilibrium with an upward age correction in the order of 100 k.y. (Schärer, 1984; Crowley et al., 2007), which is often comparable to the measured analytical uncertainty. All samples returned ages within the limit of initial Th/U disequilibrium detection, so this correction was applied to all samples for maximum U-Pb dating accuracy. Correction of ^{206}Pb/^{238}U dates for the ^{206}Pb deficit requires estimates of Th/U concentration in the zircon and Th/U concentration of the magma as the source of zircon, together with the measured radiogenic ^{206}Pb and ^{238}U (Schärer, 1984). While Th and U concentrations of zircon were obtained as part of the analytical routine, the initial Th/U concentration of the magma is more difficult to estimate and has a larger effect on the age correction (Crowley et al., 2007). Following the procedures of Holm et al. (2013), we employ the U and Th contents determined from bulk rock analysis. Uncertainties associated with the correction were propagated into errors on the corrected ages according to Crowley et al. (2007).

There are very few inherited zircon populartions in the samples, and these are easily distinguished by age (see below). Therefore, results for each sample were filtered to obtain the youngest concordant age population to be representative of the magmatic crystallization age. The effect of common Pb is taken into account by the use of Tera-Wasserburg Concordia plots (Tera and Wasserburg, 1972; Jackson et al., 2004). Spot ages were corrected for common Pb by utilizing the Age7Corr and AgeEr7Corr algorithms in Isoplot/Ex version 4.15 (Ludwig, 2009), and using the y-intercept and

corresponding sigma errors returned from the Tera-Wasserburg plots of concordant zircon populations. Weighted mean $^{206}Pb/^{238}U$ age calculations were carried out using Isoplot. All errors were propagated at 2σ level and reported at 2σ and 95% confidence for concordia and weighted averages, respectively.

Laser ablation analyses of zircons for Lu–Hf isotopes were carried out at the Advanced Analytical Centre, JCU, using a GeoLas193-nmArF laser and a Thermo-Scientific Neptune multicollector ICP-MS following the set-up outlined in Nærra et al. (2012) and Kemp et al. (2009). Zircon crystals for isotopic analysis were selected on the basis of U-Pb dating results and ablation was carried out at a repetition rate of 4 Hz and a spot size of 60 μm. All $^{176}Hf/^{177}Hf$ ratios for standard and sample zircons were normalized to measurements of the Mud Tank reference zircon (average measured $^{176}Hf/^{177}Hf$ ratio during the course of this study was 0.282493 ± 8, n=14, normalized to solution value of 0.282507) and compared with the FC1 secondary zircon standard ($^{176}Hf/^{177}Hf$ normalized = 0.282167 ± 10; Kemp et al., 2009). Epsilon Hf values for the data were calculated using the $^{206}Pb/^{238}U$ magmatic crystallization age data from the corresponding U-Pb ablation spot, and used a decay constant for ^{176}Lu of 1.867×10^{-11} y^{-1} (Söderlund et al., 2004).

4. RESULTS

4.1 Textures and U-Pb Geochronology of Zircon

Zircon crystals extracted from Kokofimpa tonalite samples (BKDD22 472, 511 and 560), are generally 100–200 μm long, euhedral stubby to prismatic crystals that

typically have bright oscillatory CL zoning with a uniform CL dark core (Fig. 2). Zircon crystals from Kokofimpa dacite samples have more variable characteristics. Zircon crystals from sample BKDD22 546 are euhedral and prismatic and are ~100–150 μm in length. They generally exhibit highly cathodoluminescent cores and oscillatory CL zoning. Zircons from samples BKDD22 582 and KKS01 have similar crystal morphologies, but are highly variable in size (100 to 1000 μm in length). Oscillatory zoning with CL bright uniform cores is typical of both zircon populations, with few crystals exhibiting complex CL zoning. Crystals are typically euhedral and prismatic with aspect ratios generally around 1:2.5. Th/U of zircon of all sample sets range between 0.5 and 1.1 (Fig. 3a).

Zircon yields from both of the Wamum tonalite samples (BWDD4 482 and 585) were low compared with the Kokofimpa samples. The Wamum zircon crystals did not exhibit a uniform set of CL imaging characteristics, but instead are marked by complex zoning patterns with only minor oscillatory zoning (Fig. 2). The crystals vary from stubby to elongate in shape and are typically between 100 and 200 μm in length, although some larger crystals are present, and many are broken or fractured. Where cores are present they have either uniform dark CL intensity, or exhibit simple, high CL contrast zoning. Some zircon crystals preserve evidence for minor dissolution with irregular crystal boundaries, but these zones were avoided during U-Pb age dating. The average Th/U ratio of the Wamum zircons is 0.80 ± 0.30.

U-Pb zircon ages corrected for common Pb and initial Th disequilibrium for selected tonalite and dacite phases from both Wamum and Kokofimpa are reported in Table 2. Nearly all analyses from each sample returned very similar ages; there was no

evidence for significant isotopic disturbance or mixing of different age domains during zircon ablation, nor was there any significant difference in the age of zircon cores and rims (Fig. 2). Coupled with the euhedral, oscillatory-zoning CL textures and relatively high U/Th ratios (Fig. 2 and 3a; e.g. Ahrens et al., 1967; Heaman et al., 1990; Corfu et al., 2003; Hoskin and Schaltegger, 2003), we interpret these data to reflect magmatic crystallization ages. We see no evidence for any secondary zoning or alteration of the zircon (e.g. Hay and Dempster, 2009) at the ablation sites chosen for analysis (see supplementary data). Corresponding concordia and weighted average plots for these data are shown in Figure 4. The weighted average age and concordia age results agree well in all cases, so henceforth we only cite the concordia ages of the samples. Complete zircon isotopic data can be found in the supplementary material. Returned ages of all samples fall within the Middle–Upper Miocene (12–6 Ma). Foliated tonalite porphyries of the Wamum porphyry prospect, BWDD4 482 and BWDD4 585, returned the oldest ages at 11.88 ± 0.13 Ma and 12.08 ± 0.13 Ma, respectively. These samples are interpreted to represent a single intrusive event, as they share similar mineralogical and petrographic characteristics and their ages are within uncertainty of each other.

Rocks types of the Kokofimpa prospect yielded a greater spread in ages between 9.4 and 6.2 Ma. The tonalites are the older phases of the intrusive complex at 9.41 ± 0.17 Ma (BKDD22 472), 8.79 ± 0.24 Ma (BKDD22 560) and 8.70 ± 0.19 Ma (BKDD22 511). The latter two ages are within uncertainty of each other, and are suggested to belong to the same intrusive event. Dacite rock types from Kokofimpa represent younger igneous suites; sample BKDD22 546 returned an age of 7.38 ± 0.18 Ma, while BKDD22 582 and KKS01 yielded similar ages of 6.28 ± 0.10 Ma and 6.20 ±

0.10 Ma, respectively.

A small proportion of the analyzed zircons returned ages of Late Permian to Middle Cretaceous ages (see supplementary material). We interpret these zircons to represent an inherited component to these magmas, which provides evidence that these magmas underwent crustal assimilation prior to emplacement.

4.2 Geochemistry

4.2.1 Major and Trace Elements

Major and trace element composition of all analyzed samples are given in Table 3. Loss on ignition (LOI) values of up to and over 5% (Table 3; Fig. 5) indicates that alteration has significantly affected many of the analyzed samples, but no clear trends between LOI and mobile elements are evident (Fig. 5). Harker variation diagrams have been used to show major element trends for all rock types from both Wamum and Kokofimpa (Fig. 6). SiO_2 contents (normalized for volatile-free compositions) vary from 61 to 72 wt.% (59 to 69 wt.% as measured), with other major elements (Fe_2O_3, CaO, and Na_2O; Fig. 6) following weakly defined trends of decreasing concentration with increasing SiO_2. By contrast, K_2O increases linearly with increasing SiO_2. The majority of the samples have between 2.2 and 2.8 wt.% MgO and 0.5 to 0.7 wt.% TiO_2, whereas the dacitic rock types have around ~1.0 wt.% MgO and ~0.35 wt.% TiO_2.

Trace element data are presented in Figures 7 and 8 by way of normalized multi-

element plots and selected incompatible element abundances and ratios, respectively. All samples from the Wamum and Kokofimpa prospects exhibit subduction-related geochemical affinities with negative Nb and Ti anomalies and relative enrichments in large-ion lithophile elements (LILE), Th, U, Pb and Sr, although the latter anomalies may in part be a consequence of alteration. All samples feature light rare earth element (REE) –enriched REE patterns (Fig. 7). Tonalite and dacite rock types from Kokofimpa generally show similar levels of LREE enrichment (Fig. 8h) and are more enriched compared with Wamum rock types. Dacitic rocks of the Kokofimpa prospect are also distinguished by distinct HREE depletion (Fig. 7c, and 8g). High field strength elements (HFSE; Ti, Zr, Hf, Nb) are variable in content and are marked by non-linear trends with regard to time. The Kokofimpa tonalites are significantly enriched in REE, Zr, Nb and Th relative to the Wamum and Kokofimpa dacite samples (Fig. 8). Two of three early tonalite phases of the Kokofimpa prospect have minor negative Eu anomalies (Fig. 7b; Eu/Eu* = 0.63 and 0.72), while both tonalite samples from Wamum have minor positive Eu anomalies (Fig. 7b; Eu/Eu* = 1.18 and 1.10).

4.2.2 Hf Isotopes

Selected zircons from samples BWDD4 585, BKDD22 472, 511, 545 and 582 were analyzed for Lu-Hf isotopic ratios. Samples were selected to represent all intrusive phases from both Wamum and Kokofimpa as established by U-Pb dating. Results are reported in Table 4 and Figures 2 and 3. Most εHf values from both the tonalite and dacite phases of Kokofimpa fall within a tight range of between 6 and 7 (Fig. 3b), with representative averages of between 6.4 and 6.8. Wamum tonalite samples, by

comparison, have a much wider range of zircon εHf values of between 8.4 and 13.2.

4.2.3 Metal Content

Assay data for Cu, Au and Mo content for rock types of the Kokofimpa prospect (Barrick Australia, unpub. data; see supplementary material) illustrates that Cu generally shows a good correlation with both Au and Mo content. Tonalite rock types have higher metal contents compared to the dacite samples. The early tonalite intrusives only contain low levels of mineralization while later tonalites generally have the highest metal grades. These trends are consistent with observed mineralogy, as sulfide mineralization is found primarily as disseminated pyrite ± chalcopyrite in tonalite samples BKDD22 511, 560 and 658. Samples from the Wamum prospect are unmineralized.

5. DISCUSSION

5.1 Geochronology and Geochemistry of the Late Miocene Maramuni arc

From the eleven samples utilized in this study we recognize three distinct episodes of magmatism at ca. 12 Ma, 9.4 - 8.7 Ma and 7.4 - 6.2 Ma based on petrography, U-Pb age dating and geochemistry results. The earliest intrusive event is represented by foliated tonalite porphyries from the Wamum prospect that formed ca. 12 Ma. Early intrusive activity at Kokofimpa comprises porphyritic tonalites; an early intrusive phase at ~9.4 Ma (samples BKDD22 472 and BKDD22 468 and 475); and a later tonalite intrusion at ~8.7 Ma, represented by samples BKDD22 511, 560 and 658.

Two subsequent episodes of porphyritic dacite emplacement occurred at 7.4 Ma and 6.2 Ma forming the latest magmatic episode in this study. Collectively, the U-Pb geochronology presented here spans the Late Miocene period in Papua New Guinea, which is marked by growth of the New Guinea Orogen from initial orogenesis at 12 Ma until renewal of orogenic activity at approximately 6 Ma (Hill and Raza, 1999; Cloos et al., 2005).

All of the samples examined here have subduction-related geochemical signatures (Fig. 7a), but further insight into the evolution of Maramuni arc magmatism in the Late Miocene may be gained from more detailed evaluation of the geochemical and isotopic compositions of the sample suite. However, we first evaluate aspects of magma differentiation of the samples and the potential of element mobility due to hydrothermal alteration, as these processes may account for some geochemical characteristics of the rocks. To assess fractionation, we use the common differentiation index of MgO content. The porphyritic tonalites from both the Wamum and Kokofimpa prospects and the early porphyritic dacite phase all have similar MgO contents (2.2–2.8 wt.%; Fig. 6), which indicates that magma differentiation will not be a major contributing factor to geochemical variation in these samples. In contrast, the late porphyritic dacite of Kokofimpa have lower MgO contents of 1–1.2 wt.%, and hence, are interpreted to be relatively evolved.

Alteration has affected all of the samples to varying extents, so we do not examine the LILE (K, Rb, Cs) or Sr in detail in terms of petrogenetic signatures, as these elements are easily mobilized during alteration. Instead, we focus on HFSE (Nb, Ti, Zr, Hf), REE and Th that have been shown to be relatively immobile under a range of

hydrothermal conditions (e.g. Floyd and Winchester, 1978), and the different intrusive phases can be distinguished by the content of these trace elements (Figs. 7 and 8). The Kokofimpa dacite suites have different MgO contents (and hence are variably fractionated), but they share similar trace element compositions, so we regard magmatic differentiation to have little influence on the trace element signatures of these rocks. Rather, we propose that the differences in trace element geochemistry between the igneous suites reflect differences in the origin and source of these magma suites.

In general, the Wamum and Kokofimpa tonalites have similar LREE-enriched REE patterns (Fig. 7b) that are typical of high-K calc-alkaline magmas (Gill, 1981). Wamum samples exhibit a slight positive Eu anomaly, which indicates these rocks have accumulated some plagioclase. The Kokofimpa tonalites feature slight negative Eu anomalies that are attributed to minor plagioclase fractionation, but they also feature higher Ce/Yb, and higher Th, REE and HFSE contents than the Wamum tonalites (Fig. 8). As outlined above, we do not regard these latter compositional differences to be due to effects of fractionation or alteration; rather we interprete these differences to be indicative of magmatic source variations. Previous work has established that arc magmas with enrichment in HFSE, Th and LREE relative to HREE, as seen in the Kokofimpa tonalites, are associated with a greater contribution of crustal material to the magma (e.g. DePaolo, 1981; Hildreth and Moorbath, 1988; Barbarin, 1999; Woodhead et al., 2010; Spandler and Pirard, 2013) that can either be derived from the subducting plate or assimilated from the arc crust during ascent of the magma. Support for crustal assimilation also comes from the presence of inherited zircons of Permian to Cretaceuous age within the samples.

Hafnium isotopic evidence further supports an interpretation for a change in crustal contribution between the tonalite samples of Wamum and Kokofimpa. A shift from relatively high positive εHf values from the Wamum tonalites to less positive εHf values in the Kokofimpa tonalites (Fig. 3b) is attributed to a shift towards more crustal values and is indicative of increased crustal input (e.g., Belousova et al., 2006; Kemp et al., 2007). Zircons from the Wamum sample show a range of εHf values and variable Th/U (Fig. 3a) that are attributed to variable degrees of assimilation of the arc crust by this magma suite. Preservation of this isotopic and compositional heterogeneity in zircon would indicate that crustal assimilation occurred soon before magma emplacement, and so is likely due to assimilation of upper crustal material, such as the Goroka and Bena Bena Formations. We expect that the highest εHf values of this sample of ~ +13 most closely represent the parental magma, as these values are typical of MORB and mantle-derived arc magmas (Fig. 9; Pearce et al., 1999).

The Kokofimpa dacites have clear subduction-related trace element patterns, but are distinct in composition from the earlier tonalite suites. The REE patterns of the dacites are again LREE enriched, but also feature prominant HREE depletion (Fig. 7c) that is most readily attributed to melt generation in the presence of garnet or fractionation of garnet, as also seen in adakitic rock types (e.g. Macpherson et al., 2006; Davidson et al., 2007; Richards, 2011). The Kokofimpa dacites do not satisfy the criteria to be defined as adakites (e.g. relatively high Na_2O [4–5 wt.%], high Sr ≥400 ppm, and elevated Al_2O_3 [≥15 wt.%]; Defant and Drummond, 1990; Macpherson et al., 2006; Richards, 2011), but the noteworthy similarities suggest some common parameter in the origin of the geochemical signature that is indicative of melt generation or

fractionation within the high-pressure garnet stability field. In this case, specific comparisons of trace element contents (e.g., HFSE, Th) between the tonalite and dacite suites is not particularly instructive, as the magma suites likely experienced very different evolutional histories (e.g. high pressure versus low pressure evolution). Nevertheless, εHf values of zircon remain a faithful monitor of crustal input, and the Kokofimpa dacites and tonalites have similar εHf values of 6–7 (Fig. 3 and 9). Unlike the Wamum sample, each of the Kokofimpa samples are internally homogenous, as they generally have a tight range in zircon εHf and Th/U (Fig. 3a). Therefore, we interpret the Hf isotope signature of the Kokofimpa samples to reflect the nature of deep crustal or mantle sources, rather that late-stage upper crustal assimilation.

To summarize, we interpret three main phases in the evolution of the Maramuni arc in the eastern Papuan Highlands. At ca. 12 Ma Wamum tonalite intrusives appear to represent 'normal calc-alkaline' arc magmatism related to subduction processes, albeit with variable εHf values indicating variable extents of assimilation of the upper crust. Two phases of tonalite emplacement at Kokofimpa are identified at 9.4 Ma and 8.7 Ma; the latter is the main mineralized phase at Kokofimpa. An increase in the crustal contribution to magma composition at this time is interpreted from elevated HFSE + Th contents, elevated LREE/HREE and less positive εHf values. The similar εHf values of +6 to +7 across all of the Kokofimpa suites is towards the lowest values for arc magmas globally (Fig. 9). Relatively low εHf of arc magmas is usually attributed to a crustal component from the slab (e.g., Pearce et al., 1999), but such signatures may also be attained by crustal assimilation during migration or ponding of the magma in the arc crust (e.g., Buys et al., 2014). Nevertheless, the lack of HREE depletion in any of the earlier rock suites indicates that melting of garnet bearing

rocks or garnet fractionation was not implicated in their evolution. Porphyritic dacites emplaced at Kokofimpa at 7.2 Ma and 6.4 Ma are devoid of mineralization, but may have been the source of fluids and metal for mineralization in the earlier Kokofimpa instrusive rocks. The HREE-depleted composition of the late dacites are, however, indicative of melt generation or fractionation at high-pressure in the presence of garnet. This temporal change in arc magma composition signals a dramatic change in sub-arc geodynamic processes between 9 and 7 Ma.

5.2 Geodynamic evolution of the Maramuni arc

We now integrate our interpretations of the Late Miocene evolution of the Maramuni arc with previously published geological data to formulate a preferred regional tectono-magmatic model for Papua New Guinea. Early Maramuni arc calc-alkaline magmatism from the Late Oligocene through to the Middle Miocene intrudes the New Guinea Mobile Belt and comprises magmatism of felsic-intermediate to mafic composition (Fig. 1 and 10). Evidence for the nature of this early arc activity, however, is sparsely exposed at the surface as mentioned above. While this study offers no further insight into the nature of early Maramuni arc activity, the previous work carried out on the early arc magmatism - although limited - does provide a context for the later arc evolution.

From approximately 12 Ma and coincident with the start of the Late Miocene there is a profound change in the tectonics of Papua New Guinea marked by onset of the New Guinea Orogen. This coincides with a change in the nature of Maramuni arc magmatism with a distinct southward migration of the arc front from the New Guinea

Mobile Belt into the Papuan Fold and Thrust Belt (Fig. 1). However, before we discuss the geodynamics for this period we must first construct a tectonic framework that holds true to the observed tectono-magmatic phenomena of both the Maramuni arc and New Guinea Orogen. The process of orogenesis can be non-unique as to the triggering mechanism; in this scenario either an episode of arc-continent collision from the north (Trobriand trough; Davies, 1990; Abbott et al., 1994; Hill and Raza, 1999) or collision of the Australian continent from the south (Pocklington trough; Hill and Hall, 2003; Cloos et al., 2005) are both plausible. A regional evaluation of the distribution of magmatism can be useful in discriminating subduction dynamics. This requires development of two generalized subduction models that can account for the southward migration of the arc. Firstly, migration of the arc to the south increases the distance between the magmatic front and subduction at the Trobriand trough; this requires a shallowing of the subduction angle, commonly referred to as flat-slab subduction (Gutscher et al., 2000; van Hunen et al., 2002; Rosenbaum and Mo, 2011). The alternative model of north-dipping subduction at the Pocklington trough, in contrast, requires a steepening angle of subduction by slab stagnation or roll-back as the arc migrates towards the plate boundary (e.g. Schellart, 2004; Arcay et al., 2005; Heuret and Lallemand, 2005; Lallemand et al., 2005; Schellart, 2008). Both models are feasible and reflect commonly interpreted tectonic responses to collision events. Recognition of renewal of orogenesis at 6 Ma, however, can help us to further discriminate between the models. There is no record of any further episodes of collision at either the Trobriand trough or Pocklington trough between 12 and 6 Ma to explain this later orogenesis. The model of Cloos et al. (2005) appeals to lithospheric delamination of the north-dipping subducted plate at the Pocklington trough coupled with isostatic crustal rebound to explain uplift. No such model exists for the Trobriand

trough and any subsequent subduction dynamics would be expected to hold implications for northern New Guinea, adjacent to the plate boundary, as opposed to the more distal central and southern regions of New Guinea where deformation is most apparent. Based on these simple tectonic relationships we favour a model of north-dipping subduction at the Pocklington trough to explain the tectono-magmatic relationship between Maramuni arc magmatism and development of the New Guinea Orogen.

We now return to the geodynamic evolution of Papua New Guinea in a broader context. From ca. 12 Ma the profound change in the geodynamics of Papua New Guinea is marked most dramatically by intial uplift of the New Guinea Orogen and contemporaneous southward migration of the Maramuni arc. Similar to the work of Cloos et al. (2005), we suggest that subduction-driven convergence and collision of the Australian continent with an outboard terrane is ultimately responsible for this change in tectonic regime. We propose in this scenario that the outboard terrane is the New Guinea Mobile Belt (Fig. 10). This timing for collision is further evidenced by a contemporaneous switch in sedimentation patterns in the Gulf of Papua (Tcherepanov et al., 2010). Prior to the Late Miocene, sedimentation on the northern Australian platform was characterized by carbonates; this is in contrast to siliciclastic deposition in the Aure trough (Pocklington trough) at the same time. Subsequent to continent collision, the Late Miocene to Early Pliocene is marked by cessation of sedimentation in the Aure trough coupled with the initiation of siliciclastic sedimentation in the Gulf of Papua (Pigram and Symonds, 1991; Tcherepanov et al., 2010) implicating closure of the Pocklington trough and the bypass of sediments over the continental Fly Platform. We interpret that

the Aure trough (Fig. 1) is an expression of the fossil Pocklington trough. The location of the Aure trough is significant in that it marks the lateral crustal boundary between the impinging stable Australian continent in the west and extended crust of the Coral Sea in the east, and hence represents a major structure accommodating convergence and right-lateral offset of the New Guinea Mobile Belt during Australian continental collision.

A significant increase in the crustal component of post-continent collision Maramuni arc magmatism (represented by the Kokofimpa tonalites) is attributed to subsequent underthrusting of the leading continental margin resulting from the collision (Fig. 10c). This is similar to the modern day tectonic analogue of continental crust underthrust beneath the impinging Finisterre Terrane and magmatism of the West Bismarck arc on the north coast of Papua New Guinea (Fig. 10f; Woodhead et al., 2010; Holm and Richards, 2013). The shift in εHf values (Fig. 3 and 9) cannot readily be explained by a Trobriand trough subduction model due to a lack of evidence for continental crust, or indeed, any crust older than ca. 45 Ma to the north of Papua New Guinea (Caroline and Solomon Sea plates; Gaina and Müller, 2007). By contrast, to the south of Papua New Guinea older continental crust is readily present in the northern Australian continent, which includes crustal blocks of Proterozoic to Paleozoic age (e.g. the Thomson Orogen, Etheridge Block, Coen, Yambo and Mt Isa Iniers: Blewett et al., 1998; Griffin et al., 2006; Korsch et al., 2012) that lie along strike to the south of the Papuan Highlands. In this case closure of a Jurassic–Cretaceous oceanic basin (Pocklington Sea) resulted in continental collision and underthrusting of rocks similar to those of North Queensland that subsequently contributed to the source of Maramuni arc magmatism. Inherited zircon of Late

Permian to Middle Cretaceous age provide some constraint on crustal ages implicated in the collision event.

Continental collision and underthrusting of the leading Australian continental margin beneath the outboard terrane and subsequent lock-up of the subduction zone, coupled with continued northward plate motion is proposed to have led to stagnation, buckling and overturning of the subducted slab (Fig. 10c). High slab strain rates associated with this plate geometry will invariably result in slab break-off and associated lithospheric delamination (Fig. 10d; van Hunen and Allen, 2011; Li et al., 2013). In the Maramuni arc we see this time marked by complex arc development. For example, the giant Porgera gold deposit formed at ca. 6 Ma hosted by intraplate alkalic basalts (Richards et al., 1990) within the extensive calc-alkaline and shoshonitic magmatism of the Maramuni arc, thus representing the development of discrete geochemical domains within a continuous magmatic arc. In the eastern Papuan Highlands we see the intrusion of several porphyritic dacite units at 7.2 Ma and 6.4 Ma. Unlike Porgera, these rocks are unmineralized but they do have geochemical signatures previously unseen in the Late Miocene Maramuni arc, such as marked HREE depletion. As mentioned earlier, lithospheric delamination has been interpreted to result in isostatic rebound of the overriding crust and uplift in the New Guinea Orogen, some 5–6 m.y. after intial continental collision and orogenesis (Fig. 10d; Cloos et al., 2005). Early Pliocene timing for orogenesis is further supported by apatite fission track studies from Hill and Gleadow (1989) who recognize renewed uplift and exhumation of the Papuan Fold and Thrust Belt from 5 Ma.

An array of potential tectonic environments can give rise to HREE depleted, or

'adakite-like' geochemical signatures that result from melt generation and/or fractionation within the garnet stability field (Macpherson et al., 2006; Alonso-Perez et al., 2009; Chiaradia et al., 2009; Richards, 2011). Geological scenarios that permit these conditions include garnet fractionation from a mantle-derived melt at high pressure (i.e. deep crust or mantle) or melting of a garnet-bearing source, such as eclogite or garnet amphibolite of the subducting slab or thickened arc crust (Sen and Dunn, 1994; Rapp and Watson, 1995; Macpherson et al., 2006; Richards and Kerrich, 2007; Chiaradia, 2009; Chiaradia et al., 2009; Richards, 2011). We propose several circumstances under which high-pressure melts could be generated at ca. 6 Ma in the Maramuni arc. Firstly, crustal thickening associated with orogenesis combined with complex subduction dynamics may cause ponding or stalling of magma at the base of the crust. Alternatively, given the suggested model of lithospheric delamination associated with slab breakup and detachment, tearing of the slab may allow inflow of hot asthenospheric mantle causing increased heat flow to the sub-arc environment and potentially melting the crust of the subducted plate or arc lower crust (Fig. 10d; Hildreth and Moorbath, 1988; Rushmer, 1993; Macpherson et al., 2006). Garnet fractionation from these magmas at depth prior to melt migration towards the surface would produce the high-pressure magmatic signature (Fig. 10d; Garrido et al., 2006; Macpherson et al., 2006; Alonso-Perez et al., 2009). Regardless of the specific mechanism for the origin of the HREE-depletion in the dacite suites of Kokofimpa, the timing and nature of these igneous rocks support a major change to sub-arc geodynamics from ca. 7 Ma that may be indicative of lithospheric delamination/slab break-off. Subsequent tectonic instability in both Papua New Guinea and the impinging Australian plate led to anomalous Pliocene–Quaternary magmatism in the Papuan Fold and Thrust Belt and in the stable continental crust of the Fly Platform

(Johnson et al. 1978; Johnson and Jaques 1980), however, the cause of this magmatism is beyond the scope of this study.

Papua New Guinea has been marked by further terrane collision and crustal shortening following the major continent collision event presented in the study. More recent collision at ca. 3.5 Ma resulted in overthrusting of the easternmost North Sepik arc terranes known as the Adelbert and Finisterre Terranes over Papua New Guinea from the northeast (Figs. 1 and 10; Abbott et al., 1994; Abbott, 1995; Holm and Richards, 2013). This collision is interpreted to have been caused by closure of the Solomon Sea due to subduction-driven convergence between the Australian and South Bismarck plates (Fig. 10; Abbott, 1995; Hill and Raza, 1999; Weiler and Coe, 2000; Holm et al., in prep). At present the ongoing convergence between the Finisterre Terrane and the Australian plate is accommodated by the Ramu–Markham Thrust Fault (e.g. Cooper and Taylor, 1987; Abbott et al., 1994; Pegler et al., 1995). We emphasize here that the geodynamic study presented here is quite independent of (but may be responsible for initiation of) the modern day setting of north-directed subduction of the Solomon Sea plate at the New Britain trench and extension in the Woodlark Basin to the southeast (e.g. Zirakparvar et al., 2013). However, the relationship between such geodynamic settings and major collision events in the western Pacific, such as presented in this study, will form the basis for future research.

6. CONCLUSIONS

We present a U-Pb geochronology, Hf isotope and geochemical investigation from the Middle–Late Miocene Maramuni arc of Papua New Guinea. Samples from the eastern

Papuan Highlands porphyry prospects of Wamum and Kokofimpa provide evidence for at least three major phases of magmatism at ca. 12 Ma, 9.4 - 8.7 Ma and 7.4 - 6.2 Ma. Geochemical data demonstrate a subduction related origin for these magmas, although the magma suites formed after ca. 9 Ma contain a significantly greater crustal component that the earlier magmas. Based on our new results and previously published data, we present a revised tectono-magmatic model for the evolution of Papua New Guinea reflecting a highly dynamic setting for arc magmatism that is marked by collision of the Australian continent and associated crustal thickening of the New Guinea Orogen from 12 Ma, together with underthrusting of the leading continental margin. The distinctive HREE-depleted geochemical signature of the youngest magmatic suite is interpreted to mark break-up and detachment of the subducted plate at ca. 7 Ma. These events led to isostatic crustal rebound and uplift in the New Guinea Orogen from approximately 6 Ma.

ACKNOWLEDGEMENTS

We acknowledge Barrick Australia for providing logistical support and samples. We thank R. Wormald for his assistance with U-Pb dating, J. Hammerli for assistance with Hf isotopes, G. Rosenbaum, S. Whattam and an anonymous reviewer for helpful suggestions and criticisms, and A. Collins for his editorial work on this manuscript. This work was funded by James Cook University, Townsville.

REFERENCES

Abbott, L.D., 1995. Neogene tectonic reconstruction of the Adelbert-Finisterre-New Britain collision, northern Papua New Guinea. Journal of Southeast Asian Earth Sciences 11, 33–51.

Abbott, L.D., Silver, E.A., Galewsky, J., 1994. Structural evolution of a modern arc–continent collision in Papua New Guinea. Tectonics 13, 1007–1034.

Ahrens, L.H., Cherry, R.D., Erlank, A.J., 1967. Observations on the Th-U relationship in zircons from granitic rocks and from kimberlites. Geochemica et Cosmochimica Acta 29, 711–716.

Alonso-Perez, R., Müntener, O., Ulmer, P., 2009. Igneous garnet and amphibole fractionation in the roots of island arcs: experimental constraints on andesitic liquids. Contributions to Mineralogy and Petrology 157, 541–558.

Arcay, D., Tric, E., Doin, M.-P., 2005. Numerical simulations of subduction zones: Effect of slab dehydration on the mantle wedge dynamics. Physics of the Earth and Planterary Interiors 149, 133–153.

Australian Bureau of Mineral Resources, 1972. Geology of Papua New Guinea, 1:1,000,000 map. Australian Bureau of Mineral Resources.

Australian Bureau of Mineral Resources, 1989. Geology of Markham Sheet, 1:250,000 map. Australian Bureau of Mineral Resources.

Baldwin, S.L., Fitzgerald, P.G., Webb, L.E., 2012. Tectonics of the New Guinea Region. Annual Review of Earth and Planetary Sciences 40, 495–520.

Barbarin, B., 1999. A review of the relationships between granitoid types, their origins and their geodynamic environments. Lithos 46, 605–626.

Belousova, E.A., Griffin, W.L., O'Reilly, S.Y., 2006. Zircon crystal morphology, trace element signatures and Hf isotope composition as a tool for petrogenetic modelling: Examples from eastern Australian granitoids. Journal of Petrology 47, 329–353.

Black, L.P., Kamo, S.L., Allen, C.M., Davis, D.W., Aleinkoff, J.N., Valley, J.W., Mudil, R., Campbell, I.H., Korsch, R.J., Williams, I.S., Foudoulis, C., 2004. Improved $^{206}Pb/^{238}U$ microprobe geochronology by the monitoring of trace-element-related matrix effect; SHRIMP, ID-TIMS, ELA-ICP-MS and oxygen isotope documentation for a series of zircon standards. Chemical Geology 205, 115–140.

Blewett, R.S., Black, L.P., Sun, S.-S., Knutson, J., Hutton, L.J., Bain, J.H.C., 1998. U-Pb zircon and Sm-Nd geochronology of the Mesoproterozoic of North Queensland: implications for a Rodinian connection with the Belt supergroup of North America. Precambrian Research 89, 101–127.

Buys, J., Spandler, C., Holm, R.J., Richards, S.W., 2014. Remnants of ancient Australia in Vanuatu: Implications for crustal evolution in island arcs and tectonic development of the southwest Pacific. Geology, In Press, doi:10.1130/G36155.1.

Chiaradia, M., 2009. Adakite-like magmas from fractional crystallization and melting-assimilation of mafic lower crust (Eocene Macuchi arc, Western Cordillera, Ecuador). Chemical Geology 265, 468–487.

Chiaradia, M., Müntener, O., Beate, B., Fontignie, D., 2009. Adakite-like volcanism of Ecuador: Lower crust magmatic evolution and recycling. Contributions to Mineralogy and Petrology 158, 563–588.

Cloos, M., Sapiie, B., van Ufford, A.Q., Weiland, R.J., Warren, P.Q., McMahon, T.P., 2005. Collisional delamination in New Guinea: The geotectonics of subducting slab breakoff. Geological Society of America, Special Paper 400.

Cooper, P., Taylor, B., 1987. Seismotectonics of New Guinea: a model for arc reversal following arc-continent collision. Tectonics 6, 53–67.

Corbett, G.J., Leach, T.M., Thirnbeck, M., Mori, W., Sione, T., Harry, K., Digan, K., and Petrie, P., 1994. The geology of porphyry-related mesothermal vein gold mineralisation north of Kainantu, Papua New Guinea. Proceedings of the PNG Geology, Exploration and Mining Conference 1994, Lae, Pp 113–124.

Corfu, F., Hanchar, J.M., Hoskin, P.W.O., Kinny P., 2003. Atlas of zircon textures. In: Hanchar, J. M., Hoskin, P.W.O. (Eds.), Reviews in Mineralogy & Geochemistry 53: Zircon. Mineralogical Society of America.

Craig, M.S., Warvakai, K., 2009. Structure of an active foreland fold and thrust belt, Papua New Guinea. Australian Journal of Earth Sciences 56, 719–738.

Crowhurst, P.V., Hill, K.C., Foster, D.A., Bennett, A.P., 1996. Thermochronological and geochemical constraints on the tectonic evolution of northern Papua New Guinea. Geological Society, London, Special Publications 106, 525–537.

Crowhurst, P.V., Maas, R., Hill, K.C., Foster, D.A., Fanning, C.M., 2004. Isotopic constraints on crustal architecture and Permo-Triassic tectonics in New Guinea: possible links with eastern Australia. Australian Journal of Earth Sciences 51, 107–122.

Crowley, J.L., Schoene, B., Bowring, S.A., 2007. U-Pb dating of zircon in the Bishop Tuff at the millennial scale. Geology 35, 1123–1126.

Davidson, J., Turner, S., Handley, H., Macpherson, C., Dosseto, A., 2007. Amphibole "sponge" in arc crust? Geology 35, 787–790.

Davidson, J., Wilson, M., 2011. Differentiation and source processes at Mt Pelée and the Quill; Active volcanoes in the Lesser Antilles arc. Journal of Petrology 52, 1493-1531.

Davies, H.L., 1990. Structure and evolution of the border region of New Guinea. In: Carman, G.J., Carman, Z. (Eds.), Petroleum Exploration in Papua New Guinea.

Proceedings of the First PNG Petroleum Convention, PNG Chamber of Mines and Petroleum, Port Moresby, 245–269.

Davies, H.L., 2012. The geology of New Guinea – the cordilleran margin of the Australian continent. Episodes 35, 87–102.

Davies, H.L., Lock, J., Tiffin, D.L., Honza, E., Okuda, Y., Murakami, F., Kisimoto, K., 1987. Convergent tectonics in the Huon Peninsula region, Papua New Guinea. Geo-Marine Letters 7, 143–152.

Davies, H.L., Symmonds, P.A., Ripper I.D., 1984. Structure and evolution of the southern Solomon Sea region. BMR Journal of Australian Geology and Geophysics 9, 49–68.

Defant, M.J., Drummond, M.S., 1990. Derivation of some modern arc magmas by melting of young subducted lithosphere. Nature 347, 662–665.

DePaolo, D.J., 1981. Trace element and isotopic effects of combined wallrock assimilation and fractional crystallization. Earth and Planetary Science Letters 53, 189–202.

Espi, J.O., Hayashi, K.-I., Komuro, K., Murakami, H., Kajiwara, Y., 2007. Geology, wall-rock alteration and vein paragenesis of the Bilimoia gold deposit, Kainantu metallogenic region, Papua New Guinea. Resource Geology 57, 249–268.

Floyd, P.A., Winchester, J.A., 1978. Identification and discrimination of altered and metamorphosed volcanic rocks using immobile elements. Chemical Geology 21, 291–306.

Gaina, C., Müller, D., 2007. Cenozoic tectonic and depth/age evolution of the Indonesian gateway and associated back-arc basins. Earth-Science Reviews 83, 177–203.

Garrido, C.J., Bodinier, J.-L., Burg, J.-P., Zeilinger, G., Hussain,, S.S., Dawood, H., Chaudhry, M.N., Gervilla, F., 2006. Petrogenesis of mafic garnet granulite in the lower crust of the Kohistan paleo-arc complex (northern Pakistan): Implications for intra-crustal differentiation of island arcs and generation of continental crust. Journal of Petrology 47, 1873–1914.

Gill, J.B., 1981. Orogenic Andesites and Plate Tectoncis. Springer-Varlag, Berlin.

Grant, J.N., Nielsen, R.L., 1975. Geology and geochronology of the Yandera Porphyry Copper Deposit, Papua New Guinea. Economic Geology 70, 1157–1174.

Griffin, W.L., Belousova, E.A., Walters, S.G., O'Reilly, S.Y., 2006. Archaean and Proterozoic crustal evolution in the Eastern Succession of the Mt Isa district, Australia: U-Pb and Hf-isotope studies of detrital zircons. Australian Journal of Earth Sciences 53, 125–149.

Gutscher, M.-A., Spakman, W., Bijwaard, H., Engdahl, E.R., 2000. Geodynamics of flat subduction: Seismicity and tomographic constraints from the Andean margin. Tectonics 19, 814–833.

Hall, R., 2002. Cenozoic geological and plate tectonic evolution of SE Asia and the SW Pacific: computer-based reconstructions, model and animations, Journal of Asian Earth Sciences 20, 353–431.

Hall, R., Spakman, W., 2002. Subducted slabs beneath the eastern Indonesia–Tonga region: insights from tomography. Earth and Planetary Science Letters 201, 321–336.

Hamilton, W., 1979. Tectonics of the Indonesian Region. United States Geological Survey Professional Paper 1078, 293–304.

Hay, D.C., Dempster, T.J., 2009. Zircon behaviour during low-temperature metamorphism. Journal of Petrology 50, 571-589.

Heaman, L.M., Bowins, R., Crocket, J., 1990. The chemical composition of igneous zircon suites: Implications for geochemical tracer studies. Geochimica et Cosmochimica Acta 54, 1597–1607.

Heuret, A., Lallemand, S., 2005. Plate motions, slab dynamics and back-arc deformation. Physics of the Earth and Planetary Interiors 149, 31–51.

Heyworth, Z., Turner, S., Schaefer, B., Wood, B., George, R., Berlo, K., Cunningham, H., Price, R., Cook, C., Gamble, J., 2007. ^{238}U-^{230}Th-^{226}Ra-^{210}Pb constraints on the genesis of high-Mg andesites at White Island, New Zealand. Chemical Geology 243, 105-121.

Hildreth, W., Moorbath, S., 1988. Crustal contributions to arc magmatism in the Andes of central Chile. Contributions to Mineralogy and Petrology 98, 455–489.

Hill, K.C., Gleadow, A.J.W., 1989. Uplift and thermal history of the Papuan Fold Belt, Papua New Guinea: Apatite fission track analysis. Australian Journal of Earth Sciences 36, 515–539.

Hill, K.C., Hall, R., 2003. Mesozoic-Cenozoic evolution of Australia's New Guinea margin in a west Pacific context. In: Hillis R.R., Müller, R.D. (Eds.) Evolution and Dynamics of the Australian Plate: Geological Society of Australia Special Publication 22, and Geological Society of America Special Paper 372, 265–290.

Hill, K.C., Kendrick, R.D., Crowhurst, P.V., Gow, P.A., 2002. Copper-gold mineralisation in New Guinea: tectonics, lineaments, thermochronology and structure. Australian Journal of Earth Sciences 49, 737–752.

Hill, K.C., Raza, A., 1999. Arc–continent collision in Papua Guinea: Constraints from fission track thermochronology. Tectonics 18, 950–966.

Holm, R.J., Richards, S.W., 2013. A re-evaluation of arc-continent collision and along-arc variation in the Bismarck Sea region, Papua New Guinea. Australian Journal of Earth Sciences 60, 605–619.

Holm, R.J., Spandler, C., Richards, S.W., 2013. Melanesian arc far-field response to collision of the Ontong Java Plateau: Geochronology and pertrogenesis of the Simuku Igneous Complex, New Britain, Papua New Guinea. Tectonophysics 603, 189–212.

Hoskin, P.W.O., Schaltegger, U., 2003. The composition of zircon and igneous and metamorphic petrogenesis. In: Hanchar, J.M., Hoskin, P.W.O. (Eds.), Reviews in Mineralogy & Geochemistry 53: Zircon. Mineralogical Society of America.

Jackson, S.E., Pearson, N.J., Griffin, W.L., Belousova, E.E., 2004. The application of laser ablation-inductively coupled plasma-mass spectrometry to in situ U-Pb zircon geochronology. Chemical Geology 211, 47–69.

Jicha, B.R., Singer, B.S., Brophy, J.G., Fournelle, J.H., Johnson, C.M., Beard, B.L., Lapen, T.J., Mahlen, N.J., 2004. Variable impact of the subducted slab on Aleutian island arc magma sources: Evidence from Sr, Nd, Pb, and Hf isotopes and trace element abundances. Journal of Petrology 45, 1845-1875.

Johnson, R.W., Jaques, A.L., 1980. Continent–arc collision and reversal of arc polarity: new interpretations from a critical area. Tectonophysics 63, 111–124.

Johnson, R.W., Mackenzie, D.E., Smith, I.E.M., 1978. Delayed partial melting of subduction-modified mantle in Papua New Guinea. Tectonophysics 46, 197–216.

Kemp, A.I.S., Foster, G.L., Scherstén, A., Whitehouse, M.J., Darling, J., Storey, C., 2009. Concurrent Pb-Hf isotope analysis of zircon by laser ablation multi-collector ICP-MS, with implications for the crustal evolution of Greenland and the Himalayas. Chemical Geology 261, 244–260.

Kemp, A.I.S., Hawkesworth, C.J., Foster, G.L., Paterson, B.A., Woodhead, J.D., Hergt, J.M., Gray, C.M., Whitehouse, M.J., 2007. Magmatic and crustal differentiation history of granitic rocks from Hf-O isotopes in zircon. Science 315, 980–983.

Korsch, R.J., Huston, D.L., Henderson, R.A., Blewett, R.S., Withnall, I.W., Fergusson, C.L., Collins, W.J., Saygin, E., Kositcin, N., Meixner, A.J., Chopping, R., Henson, P.A., Champion, D.C., Hutton, L.J., Wormald, R., Holzschuh, J., and Costelloe, R.D., 2012. Crustal architecture and geodynamics of North Queensland, Australia: Insights from deep seismic reflection profiling. Tectonophysics 572–573, 76–99.

Lallemand, S., Heuret, A., Boutelier, D., 2005. On the relationships between slab dip, back-arc stress, upper plate absolute motion, and crustal nature in subduction zones. Geochemistry, Geophysics, Geosystems 6, Q09006.

Li, Z.-H., Xu, Z., Gerya, T., and Burg, J.-P., 2013. Collision of continental corner from 3-D numerical modeling. Earth and Planetary Science Letters 380, 98–111.

Lock, J., Davies, H.L., Tiffin, D.L., Murakami, F., Kisimoto, K., 1987. The Trobriand subduction system in the western Solomon Sea. Geo-Marine Letters 7, 129–134.

Ludwig, K.R., 2009. User's Manual for Isoplot 3.70: A Geochronological Toolkit for Microsoft Excel. Berkeley Geochronology Center Special Publication No. 4.

Macpherson, C.G., Dreher, S.T., Thirlwall, M.F., 2006. Adakites without slab melting: High pressure differentiation of island arc magma, Mindanao, the Philippines: Earth and Planetary Science Letters 243, 581–593.

Mann, P., Taira, A., 2004. Global tectonic significance of the Solomon Islands and Ontong Java Plateau convergent zone. Tectonophysics 389, 137–190.

Marini, J.-C., Chauvel, C., Maury, R., 2005. Hf isotope compositions of northern Luzon arc lavas suggest involvement of pelagic sediments in their source. Contributions to Mineralogy and Petrology 149, 216-232.

Nærra, T., Scherstén, A., Rosing, M.T., Kemp, A.I.S., Hoffmann, J.E., Kokfelt, T.F., Whitehouse, M.J., 2012. Hafnium isotope evidence for a transition in the dynamics of continental growth 3.2 Gyr ago. Nature 485, 627–630.

Page, R.W., 1976. Geochronology of igneous and metamorphic rocks in the New Guinea Highlands. Bureau of Mineral Resources, Geology and Geophysics Bulletin 162, Australian Government Publishing Service, Canberra.

Page, R.W., McDougall, I., 1972. Ages of mineralisation of gold and porphyry copper deposits in the New Guinea Highlands. Economic Geology 67, 1034–1048.

Parrish, R.R., 1990. U-Pb dating of monazite and its application to geological problems. Canadian Journal of Earth Sciences 27, 1431–1450.

Pearce, J.A., Kempton, P.D., Nowell, G.M., Noble, S.R., 1999. Hf-Nd element and isotope perspective on the nature and provenance of mantle and subduction components in western Pacific arc-basin systems. Journal of Petrology 40, 1579-1611.

Pegler, G., Das, S., Woodhouse, J.H., 1995. A seismological study of the eastern New Guinea and the western Solomon Sea regions and its tectonic implications. Geophysical Journal International 122, 961–981.

Petterson, M.G., Babbs, T., Neal, C.R., Mahoney, J.J., Saunders, A.D., Duncan, R.A., Tolia, D., Magu, R., Qopoto, C., Mahoa, H., Natogga, D., 1999. Geological-tectonic framework of Solomon Islands, SW Pacific: crustal accretion and growth with an intra-oceanic setting. Tectonophysics 301, 35–60.

Pigram, C.J., Symonds, P.A., 1991. A review of the timing of the major tectonic events in the New Guinea Orogen. Journal of Southeast Asian Earth Sciences 6, 307–318.

Rapp, R.P., Watson, E.B., 1995. Dehydration melting of metabasalt at 8–32 kbar: Implications for continental growth and crust-mantle recycling. Journal of Petrology 36, 891–931.

Renne, P.R., Mundil, R., Balco, G., Min, K., Ludwig, K.R., 2010. Joint determination of 40K decay constants and 40Ar*/40K for the Fish Canyon sanidine standard, and improved accuracy for 40Ar/39Ar geochronology. Geochimica et Cosmochimica Acta 74, 5349–5367.

Richards, J.P., 2011. High Sr/Y arc magmas and porphyry Cu ± Mo ± Au deposits: Just add water. Economic Geology 106, 1075–1081.

Richards, J.P., Chappell, B.W., and McCulloch, M.T., 1990. Intraplate-type magmatism in a continent-island-arc collision zone: Porgera intrusive complex, Papua New Guinea. Geology 18, 958–961.

Richards, J.P., Kerrich, R., 2007. Adakite-like rocks: Their diverse origins and questionable role in metallogenesis. Economic Geology 102, 537–576.

Richards, J.P., McDougall, I., 1990. Geochronology of the Porgera gold deposit, Papua New Guinea: Resolving the effects of excess argon on K-Ar and $^{40}Ar/^{39}Ar$ age

estimates for magmatism and mineralization. Geochimica et Cosmochimica Acta 54, 1397–1415.

Ripper, I.D., 1982. Seismicity of the Indo-Australian/Solomon Sea plate boundary in the southeast Papua region. Tectonophysics 87, 355–369.

Rogerson, R., Williamson, A., 1985. Age, petrology and mineralization associated with the two Neogene intrusive types in the Eastern Highlands of Papua New Guinea. Geological Survey of Papua New Guinea Open File Report 85.

Rosenbaum, G., Mo, W., 2011. Tectonic and magmatic responses to the subduction of high bathymetric relief. Gondwana Research 19, 571–582.

Rushmer, T., 1993. Experimental high-pressure granulites: Some applications to natural mafic xenolith suites and Archean granulite terranes. Geology 21, 411–414.

Schärer, U., 1984. The effect of initial ^{230}Th disequilibrium on young U-Pb ages: the Makalu case, Himalaya. Earth and Planetary Science Letters 67, 191–204.

Schellart, W.P., 2004. Quantifying the net slab pull force as a driving mechanism for plate tectonics. Geophysical Research Letters 31, L07611.

Schellart, W.P., 2008. Overriding plate shortening and extension above subduction zones: A parametric study to explain formation of the Andes Mountains. GSA Bulletin 120, 1441–1454.

Schellart, W.P., Lister, G.S., Toy, V.G., 2006. A Late Cretaceous and Cenozoic reconstruction of the Southwest Pacific region: Tectonics controlled by subduction and slab rollback processes. Earth-Science Reviews 76, 191–233.

Schmitz, M.D., Bowring, S.A., 2001. U-Pb zircon and titanite systematics of the Fish Canyon Tuff: an assessment of high-precision U-Pb geochronology and its application to young volcanic rocks. Geochimica et Cosmochimica Acta 65, 2571–2587.

Schuth, S., Münker, C., König, S., Qopoto, C., Basi, S., Garbe-Schönberg, D., Ballhaus, C., 2009. Petrogenesis of lavas along the Solomon Island arc, SW Pacific: Coupling of compositional variations and subduction zone geometry. Journal of Petrology 50, 781-811.

Sen, C., Dunn, T., 1994. Dehydration melting of a basaltic composition amphibolite at 1.5 and 2.0 GPa: Implications for the origin of adakites. Contributions to Mineralogy and Petrology 117, 394–409.

Shedden, S.H., 1990. Wamum copper-gold prospect. In: Hughes, F.E. (Ed), Geology of the Mineral Deposits of Australia and Papua New Guinea, Pp. 1759–1761. The Australian Institute of Mining and Metallurgy, Melbourne.

Sillitoe, R.H., 2010. Porphyry copper systems. Economic Geology 105, 3–41.

Smith, I.E.M., 2013. The chemical characterization and tectonic significance of ophiolite terrains in southeastern Papuan New Guinea. Tectonics 32, 1–12.

Söderlund, U., Patchett, P.J., Vervoort, J.D., Isachsen, C.E., 2004. The ^{176}Lu decay constant determined by Lu-Hf and U-Pb isotope systematics of Precambrian mafic intrusions. Earth and Planetary Science Letters 219, 311–324.

Spandler, C., Pirard, C., 2013. Element recycling from subducting slabs to arc crust: A review. Lithos 170–171, 208–223.

Spandler, C., Pettke, T., Rubatto, D., 2011. Internal and external fluid sources for eclogite-facies veins in the Monviso meta-ophiolite, Western Alps: implications for fluid flow in subduction zones. Journal of Petrology 52, 1207–1236.

Sun, S., McDonough, W.F., 1989. Chemical and isotopic systematics of oceanic basalts: implications for mantle composition and processes. Geological Society, London, Special Publications 42, 313–345.

Tcherepanov, E.N., Droxler, A.W., Lapointe, P., Mohn, K., Larsen, O.A., 2010. Siliciclastic influx and burial of the Cenozoic carbonate system in the Gulf of Papua. Marine and Petroleum Geology 27, 533–554.

Tera, F., Wasserburg, G.J., 1972. U-Th-Pb systematics in three Apollo 14 basalts and the problem of initial Pb in lunar rocks. Earth and Planetary Science Letters 14, 281–304.

Tingey, R.J., Grainger, D.J., 1976. Markham – Papua New Guinea, 1:250,000 Geological Series with Explanatory Notes. International Index Sheet Sb/55-10. Geological Survey of Papua New Guinea, Port Moresby, 49p.

Tollstrup, D., Gill, J., Kent, A., Prinkey, D., Williams, R., Tamura, Y., Ishizuka, O., 2010. Across-arc geochemical trends in the Izu-Bonin arc: Contributions from the subducting slab, revisited. Geochemistry, Geophysics, Geosystems 11, doi:10.1029/2009GC002847.

Tosdal, R., 2009. Overview of the Kokofimpa porphyry Cu-Au prospect, Papua New Guinea. Unpublished company report, Barrick Gold.

Tucker, R.T., Roberts, E.M., Hu, Y., Kemp, A.I.S., Salisbury, S.W., 2013. Detrital zircon age constraints for the Winton Formation, Queensland: Contextualizing Australia's Late Cretaceous dinosaur faunas. Gondwana Research 24, 767–779.

Van Achterbergh, E., Ryan, C.G., Jackson, S.E., Griffin, W.L., 2001. Appendix, in: P.J. Sylvester (Ed.), Laser Ablation-ICP-Mass Spectrometry in the Earth Sciences: Principle and Applications. Mineralog. Assoc. Can. (MAC) Short Course Series, Ottawa, Ontario, Canada, 29, 239.

van Dongen, M., Weinberg, R.F., Tomkins, A.G., Armstrong, R.A., Woodhead, J.D., 2010. Recycling of Proterozoic crust in Pleistocene juvenile magma and rapid

formation of the Ok Tedi porphyry Cu-Au deposit, Papua New Guinea. Lithos 114, 282–292.

van Hunen, J., Allen, M.B., 2011. Continental collision and slab break-off: A comparison of 3-D numerical models with observations. Earth and Planetary Science Letters 302, 27–37.

van Hunen, J., van den Berg, A.P., Vlaar, N.J., 2002. On the role of subducting oceanic plateaus in the development of shallow flat subduction. Tectonophysics 352, 317–333.

Van Wyck, N., Williams, I.S., 2002. Age and provenance of basement metasediments from the Kubor and Bena Bena Blocks, central Highlands, Papua New Guinea: constraints on the tectonic evolution of the northern Australian cratonic margin. Australian Journal of Earth Sciences 49, 565–577.

Weiler, P.D., Coe, R.S., 2000. Rotations in the actively colliding Finisterre Arc Terrane: paleomagnetic constraints on Plio–Pleistocene evolution of the South Bismarck microplate, northeastern Papua New Guinea. Tectonophysics 316, 297–325.

Whalen, R.E., Britten, R.M., McDougall, I., 1982. Geochronology and geochemistry of the Frieda River Prospect Area, Papua New Guinea. Economic Geology 77, 592–616.

Whattam, S.A., 2009. Arc-continent collisional orogenesis in the SW Pacific and the nature, source and correlation of emplaced ophiolitic nappe components. Lithos, 113, 88-114.

Whattam, S.A., Malpas, J., Ali, J.R., Smith, I.E.M., 2008. New SW Pacific tectonic model: Cyclical intraoceanic magmatic arc construction and near-coeval emplacement along the Australia-Pacific margin in the Cenozoic. Geochemistry, Geophysics, Geosystems, 9, Q03021.

Woodhead J.D., Herget, J.M., Davidson, J.P., Eggins, S.M., 2001. Hafnium isotope evidence for 'conservative' element mobility during subduction zone processes. Earth and Planetary Science Letters 192, 331-346.

Woodhead, J., Hergt, J., Sandiford, M., Johnson, W., 2010. The big crunch: Physical and chemical expressions of arc/continent collision in the Western Bismarck arc. Journal of Volcanology and Geothermal Research 190, 11–24.

Zirakparvar, N.A., Baldwin, S.L., Vervoort, J.D., 2013. The origin and geochemical evolution of the Woodlark Rift of Papua New Guinea. Gondwana Research 23, 931-943.

FIGURE CAPTIONS

Figure 1. Panel A: Distribution of mapped magmatic rock units (from Australian

Bureau of Mineral Resources, 1972) and major tectonic boundaries of central Papua New Guinea. Published K/Ar (white boxes) and U-Pb ages (grey boxes) for Late Cenozoic magmatic rocks are from Page and McDougall (1972), Grant and Nielsen (1975), Page (1976), Whalen et al. (1982), Rogerson and Williamson (1985), Richards and McDougall (1990), and van Dongen et al. (2010). Panel B: Major tectonic elements of Papua New Guinea; Adelbert Terrane (AT); Aure trough (AuT); Bundi fault zone (BFZ); Bismarck Sea seismic lineation (BSSL); Fly Platform (FP); Finisterre Terrane (FT); Lagaip fault zone (LFZ); Manus Basin (MB); New Britain (NB); New Britain trench (NBT); New Guinea trench (NGT); North Sepik arc (NSA); Owen Stanley fault zone (OSFZ); Papuan Fold and Thrust Belt (PFTB); Papuan Peninsula (PP); Pocklington trough (PT); Ramu Markham fault zone (RMFZ); South Bismarck plate (SBP); Solomon Sea (SS); Trobriand trough (TT); Woodlark Basin (WB). Panel C: Regional geology of the eastern Papuan Highlands (modified from Australian Bureau of Mineral Resources, 1989).

Figure 2. Representative cathodoluminescence images, U-Pb ages and εHf values for the different intrusive phases of Wamum and Kokofimpa.

Figure 3. Plot of εHf values versus a) zircon Th/U; and b) zircon age for selected samples. Fields for metamorphic and igneous Th/U values are from Hoskin and Schaltegger (2003); all zircons analyzed hold igneous Th/U values. Values for εHf and associated averages show a decrese in εHf over time, see text for discussion.

Figure 4. Weighted average and concordia plots for selected samples. Plots are constructed from U-Pb calculated ages and isotopic compositions respectively

(detailed isotopic data in supplementary material). Tera-Wasserburg plots are corrected for initial Th disequilibrium; weighted average plots are corrected for initial Th disequilibrium and common Pb. All error bars, data-point error ellipses and calculated errors are 2σ and 95% confidence for concordia and weighted averages respectively.

Figure 5. Major and trace element variation with alteration intensity (LOI) diagrams for all samples.

Figure 6. Major element variation diagrams for all samples. Data is normalized for volatile-free compositions.

Figure 7. N-MORB normalized multi-element plot and C1 chondrite normalized REE plots for the Kokofimpa and Wamum porphyry prospects. N-MORB and C1 chondrite normalizations are from Sun and McDonough (1989).

Figure 8. Selected incompatible element variation and ratios for all samples.

Figure 9. Comparison of samples in this study with modern arcs for selected trace element ratios versus εHf. High-sediment arc field includes the Sunda arc (Woodhead et al., 2001), Lesser Antilles arc (Davidson and Wilson, 2011), and New Zealand arc (Heyworth et al., 2007); low-sediment arc field includes the Izu-Bonin and Mariana arcs (Pearce et al., 1999; Woodhead et al., 2001; Tollstrup et al., 2010); the regional West Bismarck arc (Woodhead et al., 2010) and Solomon arc (Schuth et al., 2009) are shown for comparison; other arcs fields include the Luzon arc (Marini et al., 2005)

and Aleutian arc (Jicha et al., 2004); MORB field is from Sun and McDonough (1989) and Pearce et al. (1999). Data points for this study represent average values, the range of εHf values for the Wamum tonalite are indicated.

Figure 10. Simplified geodynamic evolution of the Maramuni arc. Time steps represent: a) north-dipping subduction of the Pocklington Sea slab at the Pocklington trough and associated magmatism of the Maramuni arc intruding the New Guinea Mobile Belt (NGMB); b) onset of continental collision and growth of the New Guinea Orogen from ca. 12 Ma as the Australian continent enters the Pocklington trough. Collision between the Australian continent and the New Guinea Mobile Belt leads to cessation of subduction at the Pocklington trough and associated foundering and steepening of the Pocklington Sea slab in the mantle; c) continued orogenesis results from convergence between the Australian continent and New Guinea Mobile Belt, associated with underthrusting of the leading Australian continental margin at the Pocklington trough. Northward motion of the Australian plate relative to the foundering Pocklington Sea slab leads to buckling and overturning of the slab. A reduction in convergence at the Pocklington trough is accommodated by initiation of north-dipping subduction of the Solomon Sea plate beneath the Finisterre Terrane; d) lithospheric delamination of the Pocklington Sea slab some 6 m.y. after continental collision results in renewed orogenesis in the New Guinea Orogen, and HREE-depleted magmatism at Kokofimpa. Subduction of the Solomon Sea plate continues at the New Britain trench but also begins to underthrust the New Guinea Mobile Belt at the Trobriand trough (Holm et al., In Prep); e) Maramuni arc magmatism migrates southward into the Papuan Fold and Thrust Belt. Subduction of the Solomon Sea plate at the New Britain and Trobriand subduction systems results in closure of the

Solomon Sea and collision and overthrusting of the Finisterre Terrane above the New Guinea Mobile Belt. Magmatism of the West Bismarck arc begins northward of the Finisterre Terrane; and f) convergence between the Finisterre Terrane and New Guinea Mobile Belt continues at the Ramu-Markham fault. Underthrusting of the New Guinea Mobile Belt beneath the Finisterre Terrane results in crustal-derived magmatism in the West Bismarck arc. The foundered Solomon Sea slab is laterally continuous with the present day Solomon Sea plate to the east (see Fig. 1). Present day cross-section is modified from Holm and Richards (2013).

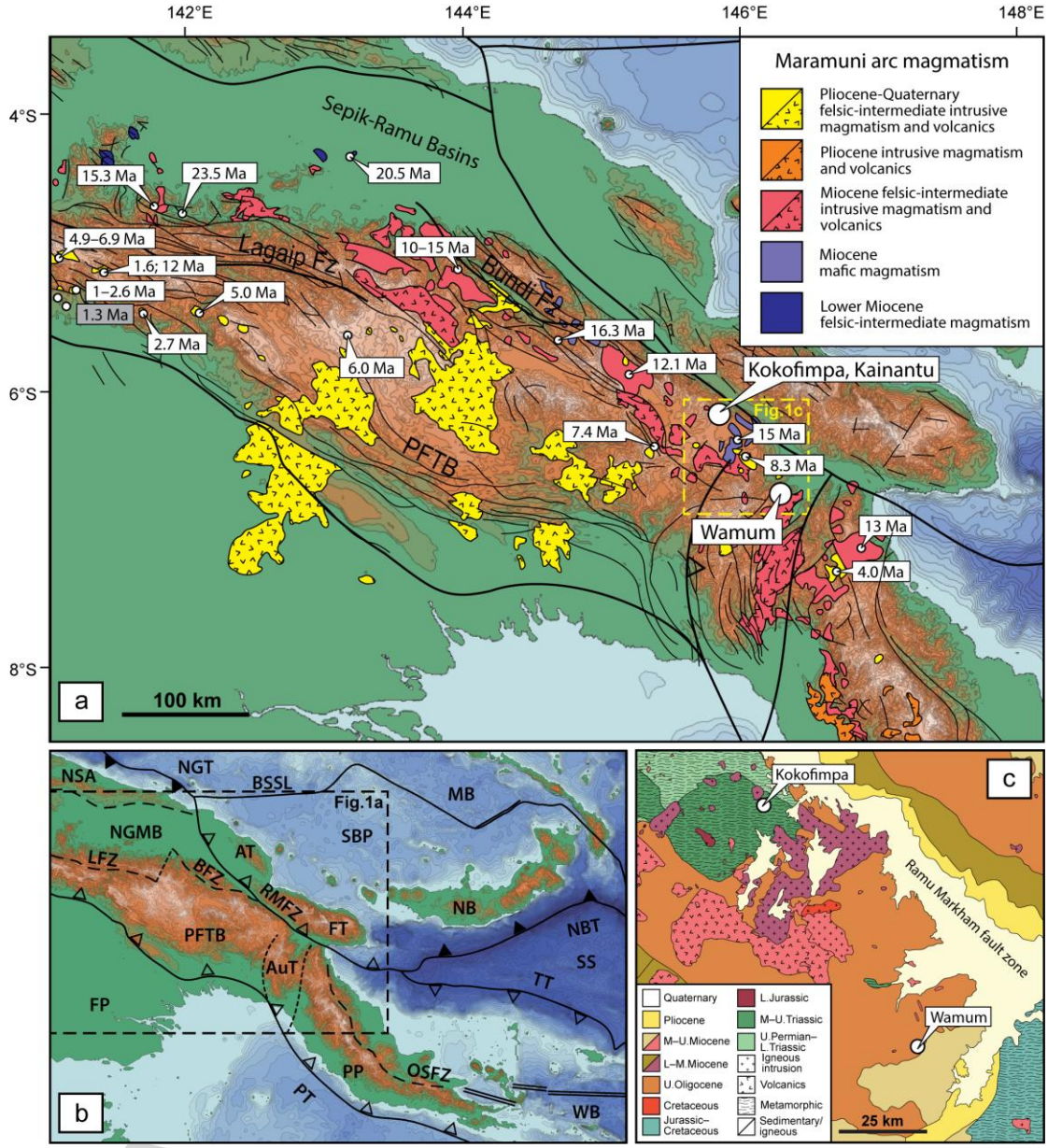

Figure 1

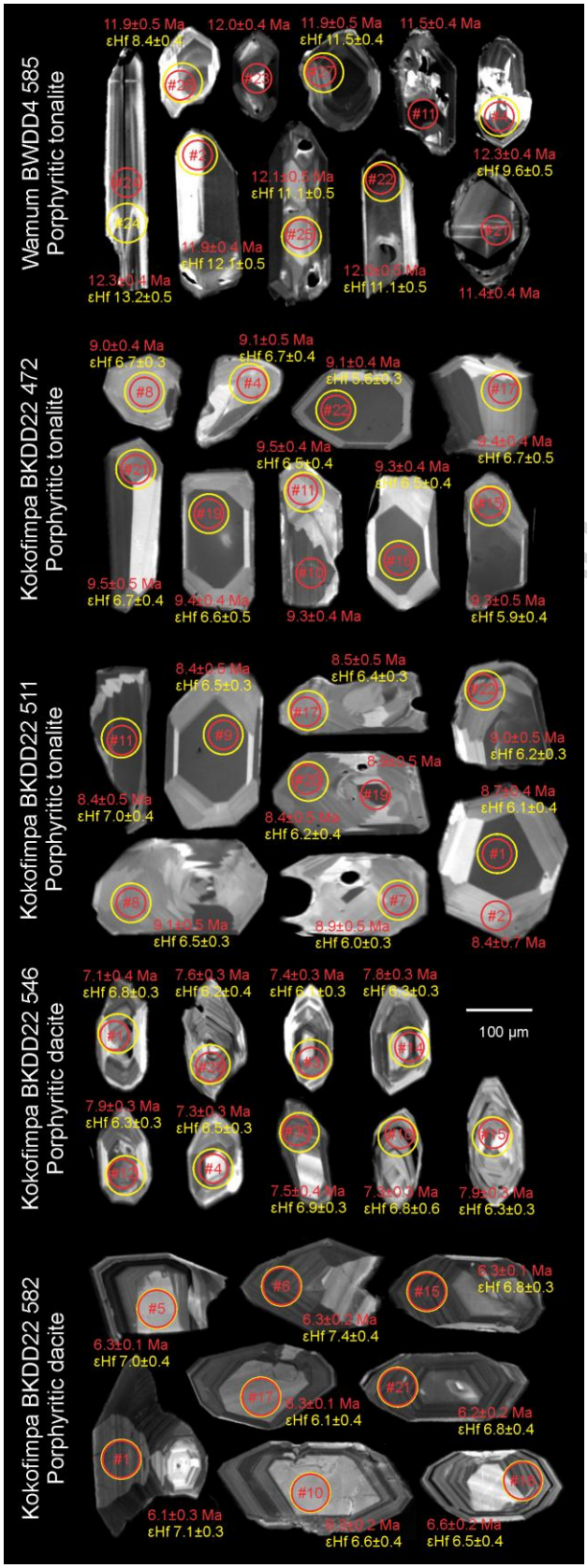

Figure 2

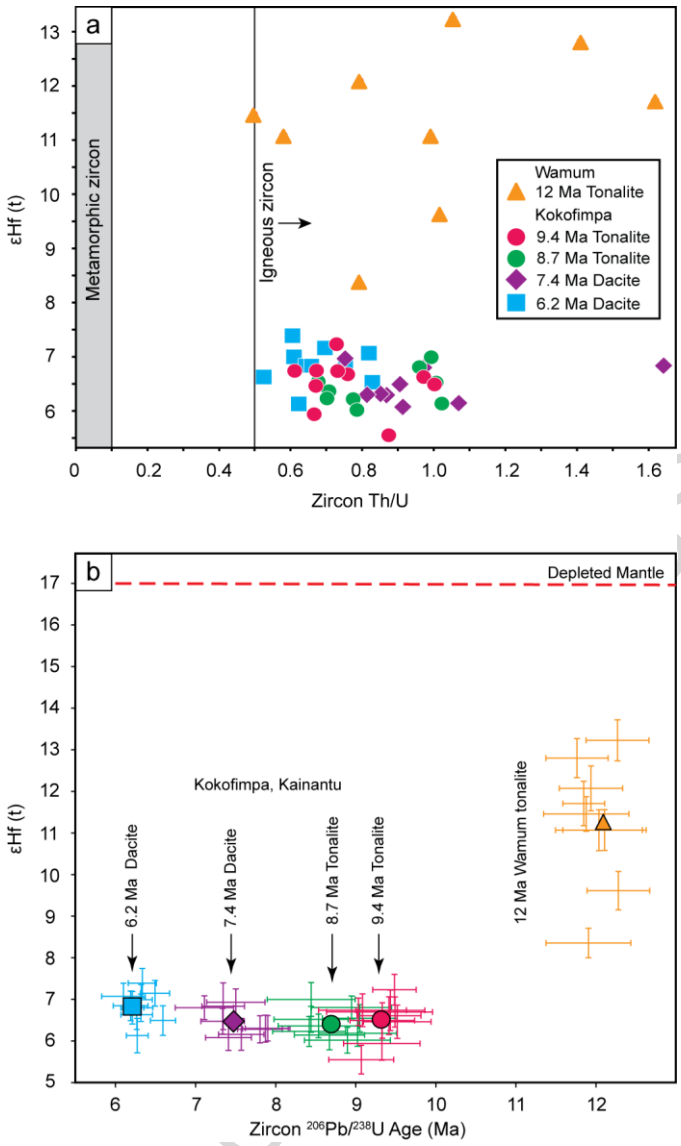

Figure 3

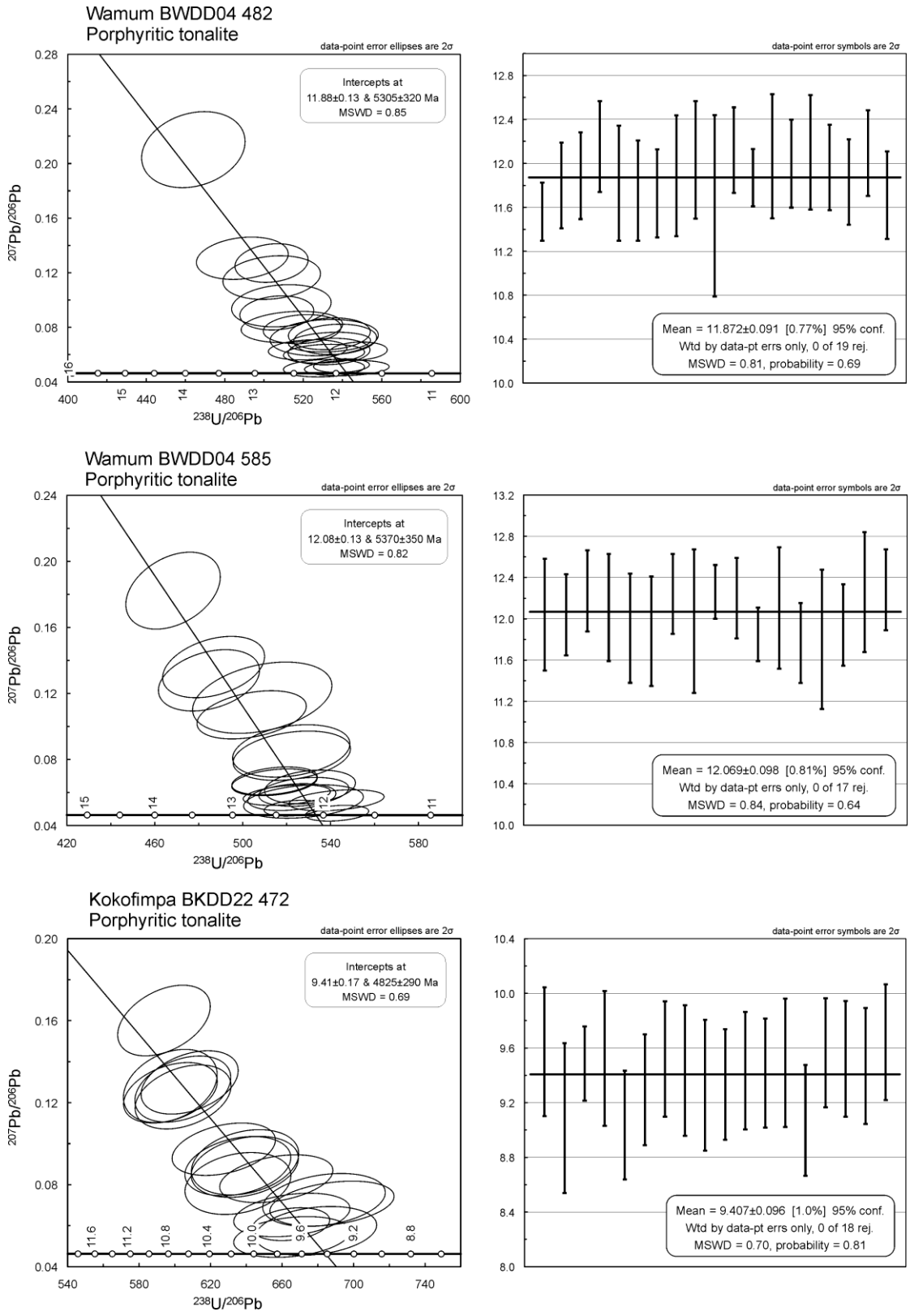

Figure 4a

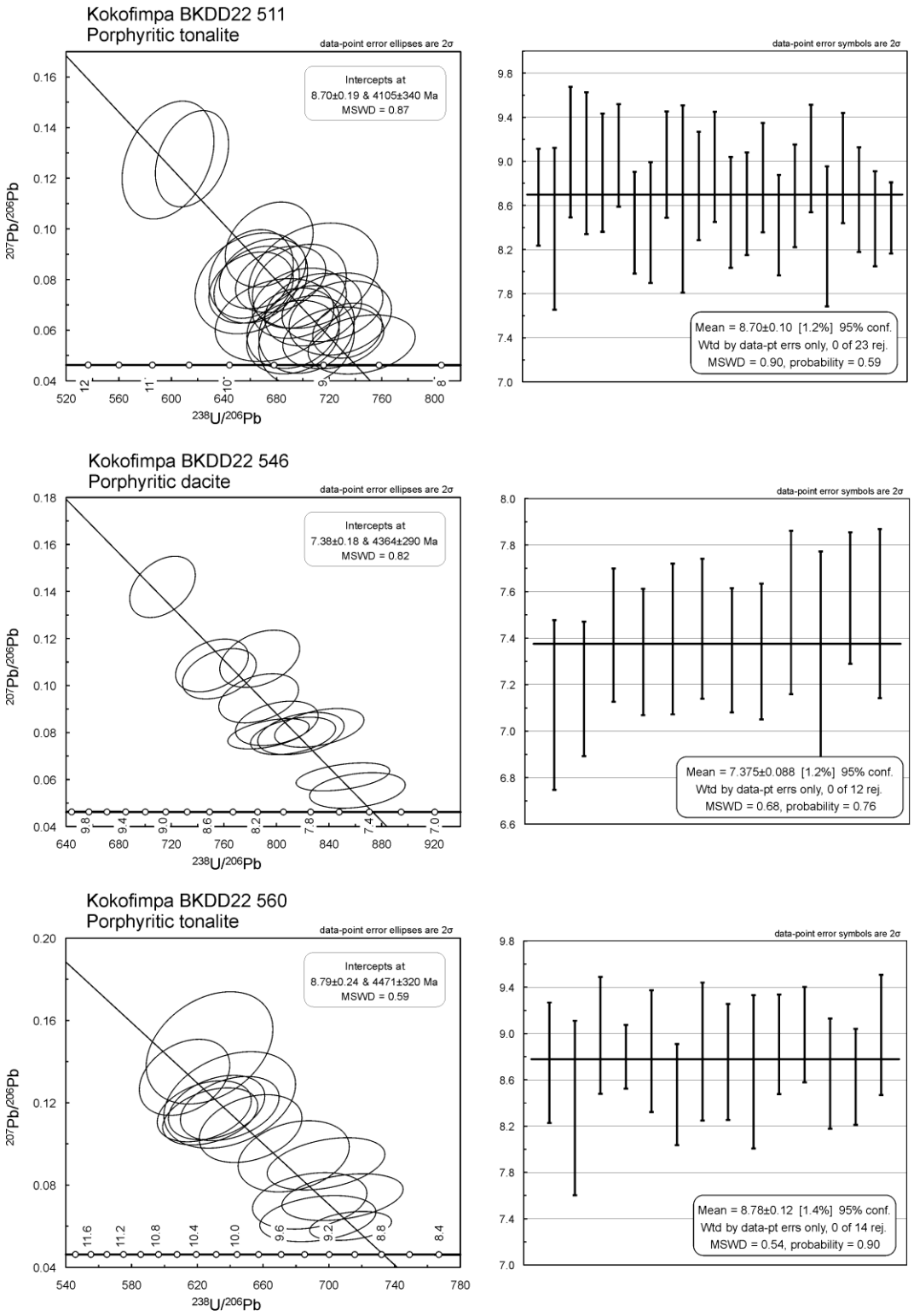

Figure 4b

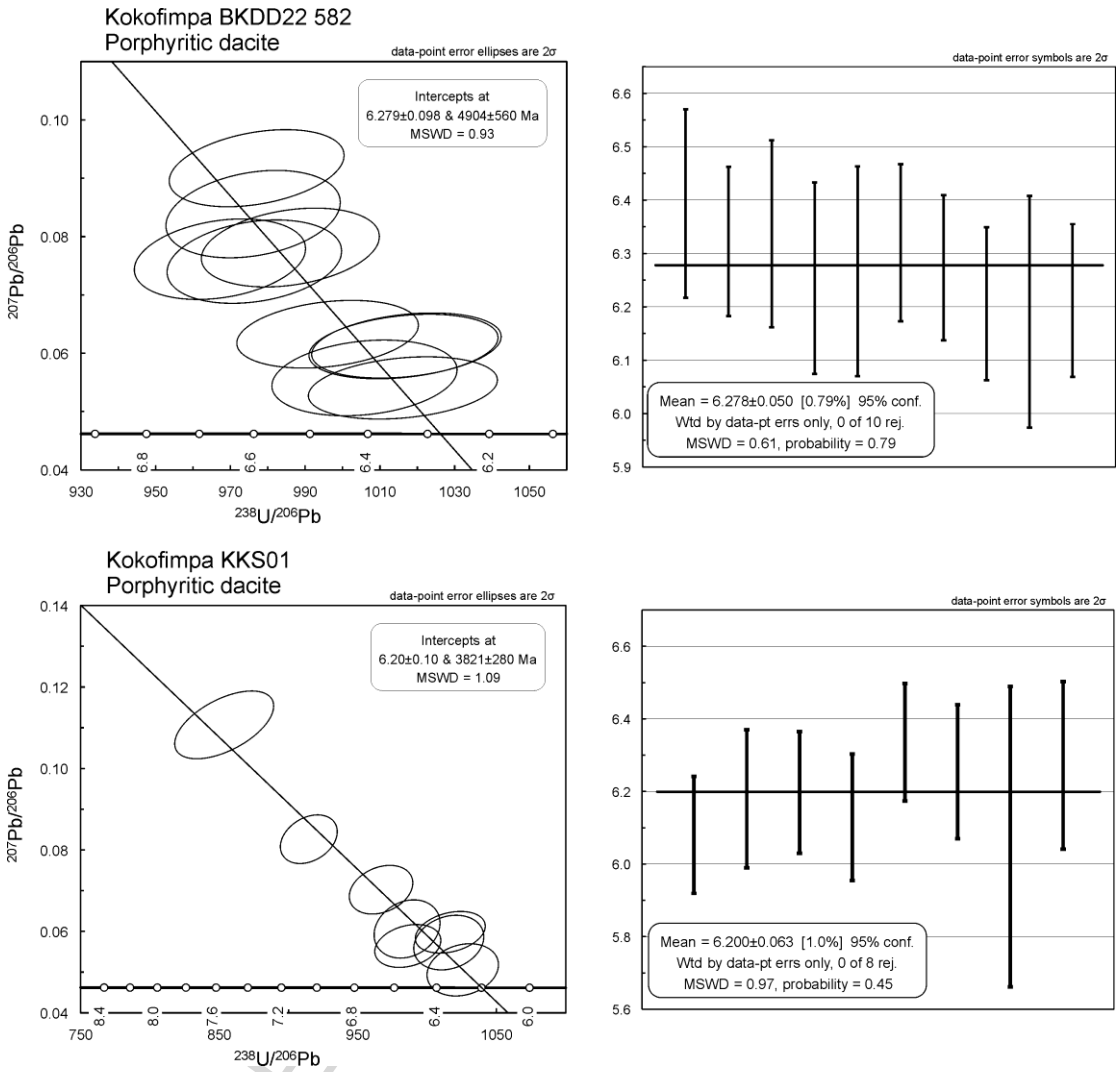

Figure 4c

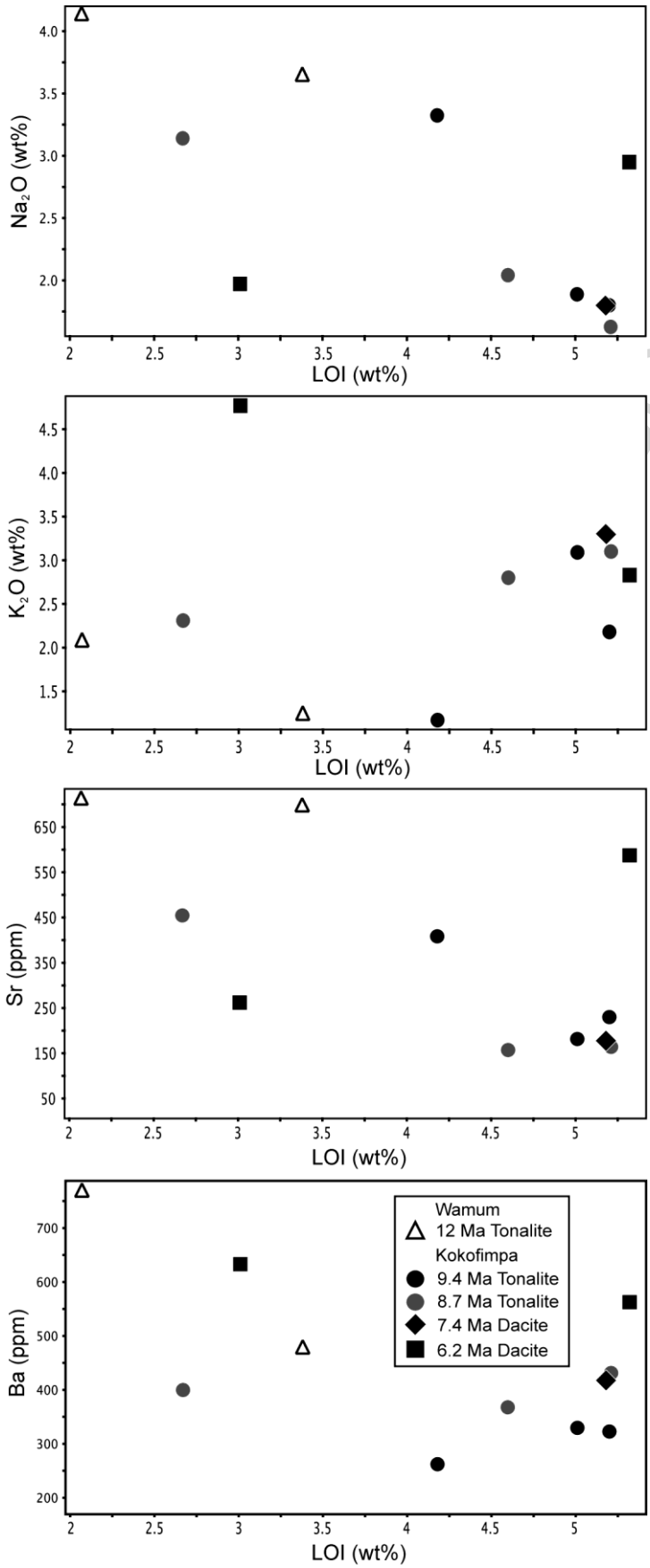

Figure 5

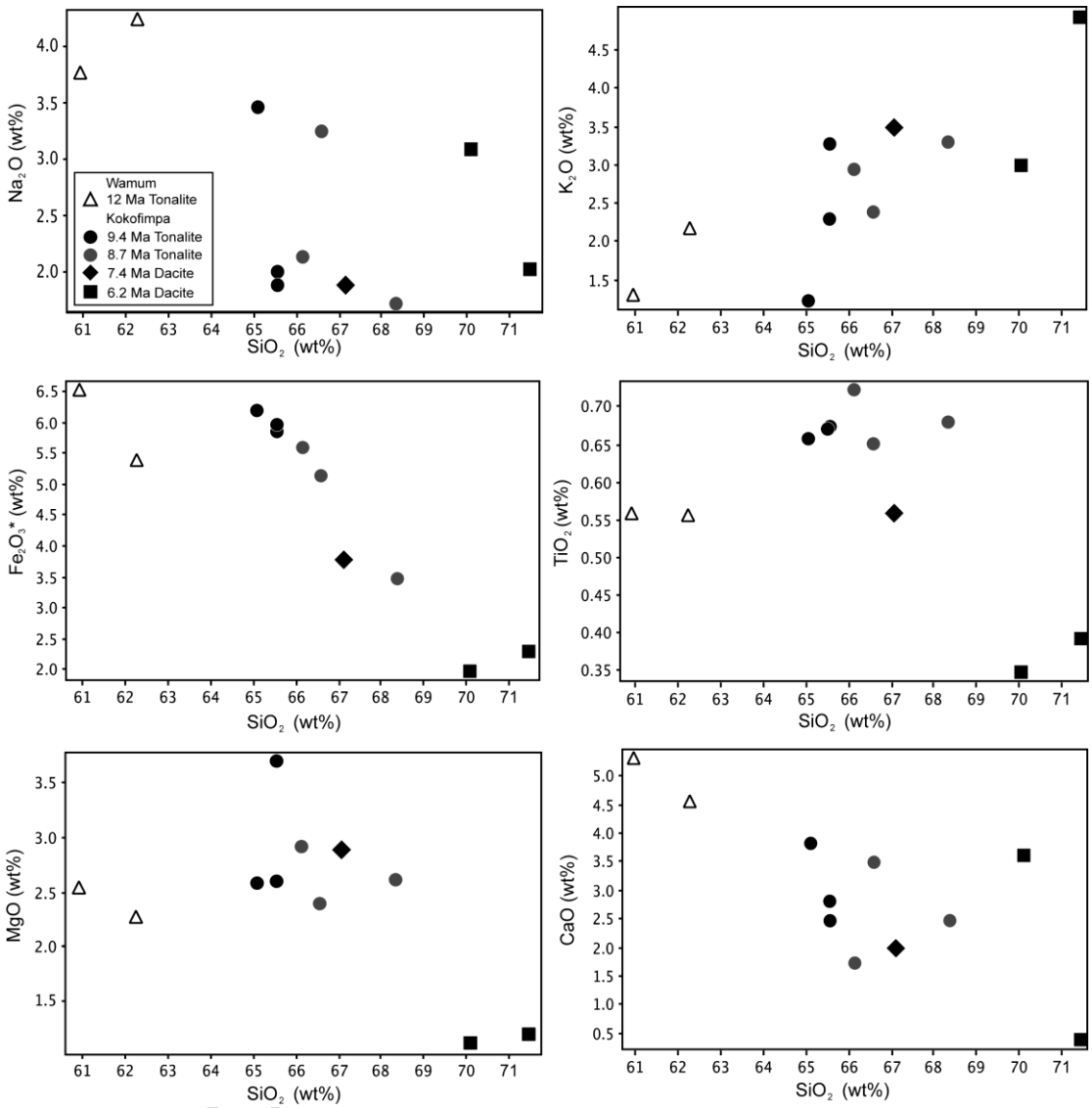

Figure 6

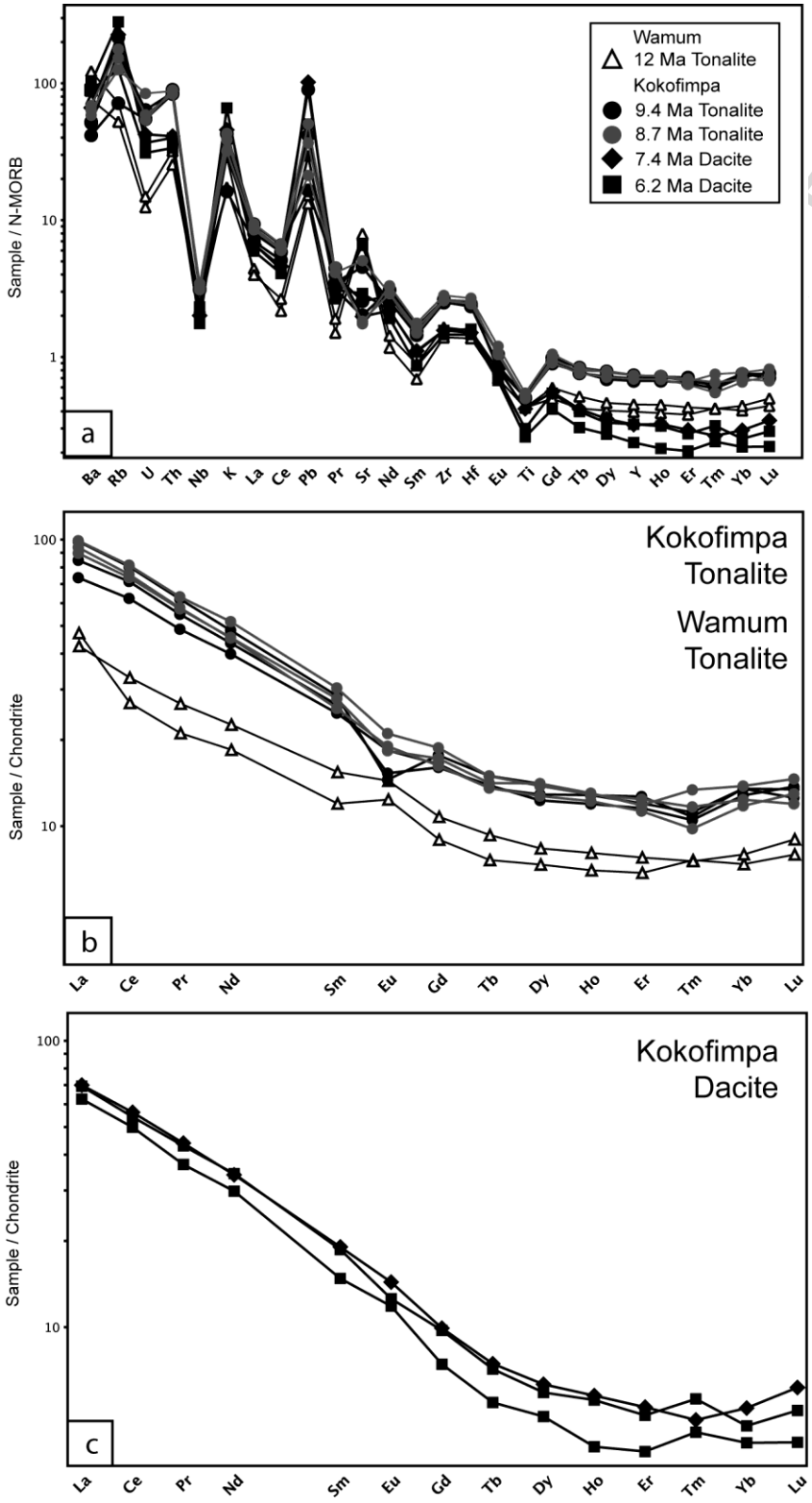

Figure 7

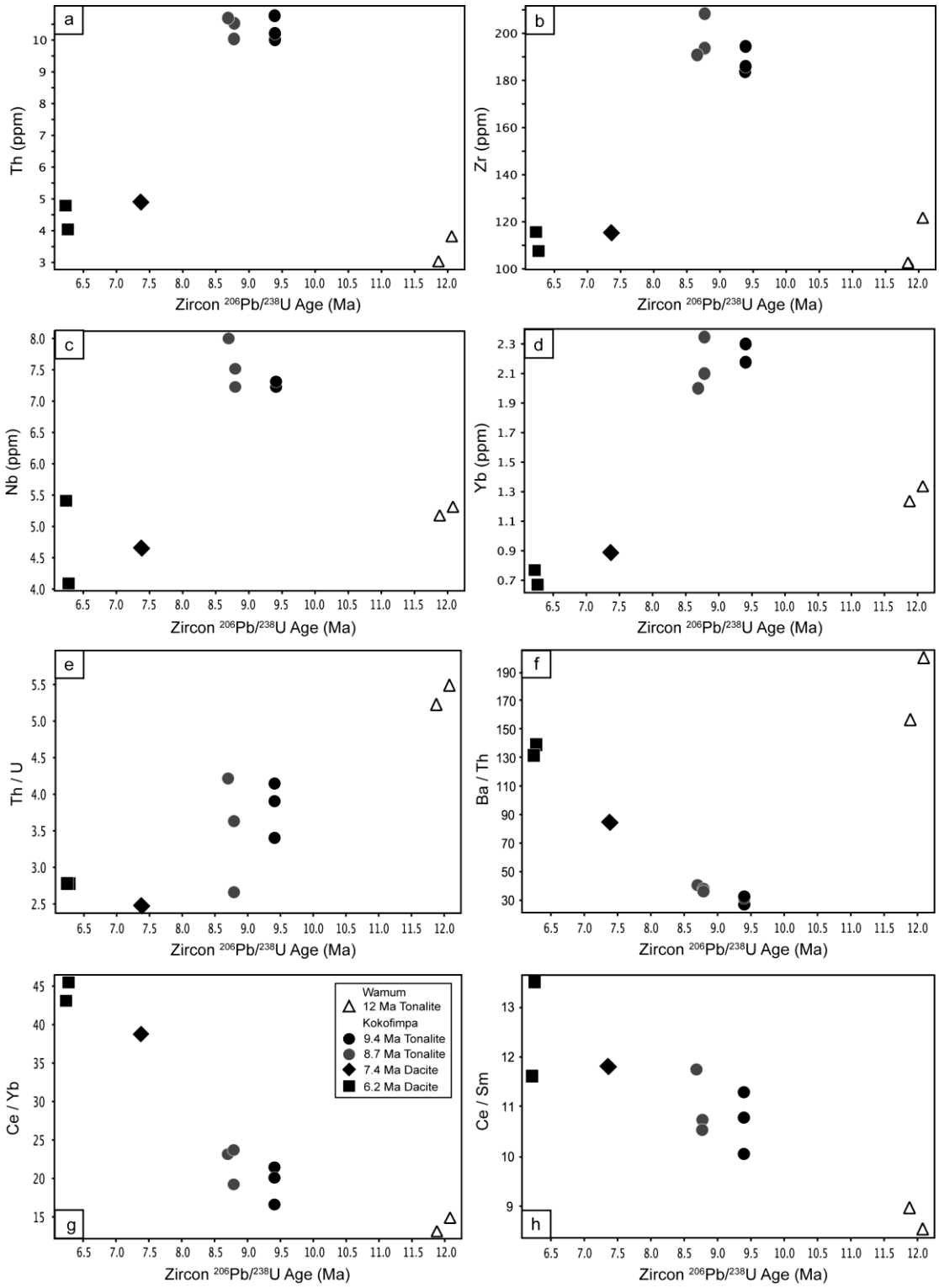

Figure 8

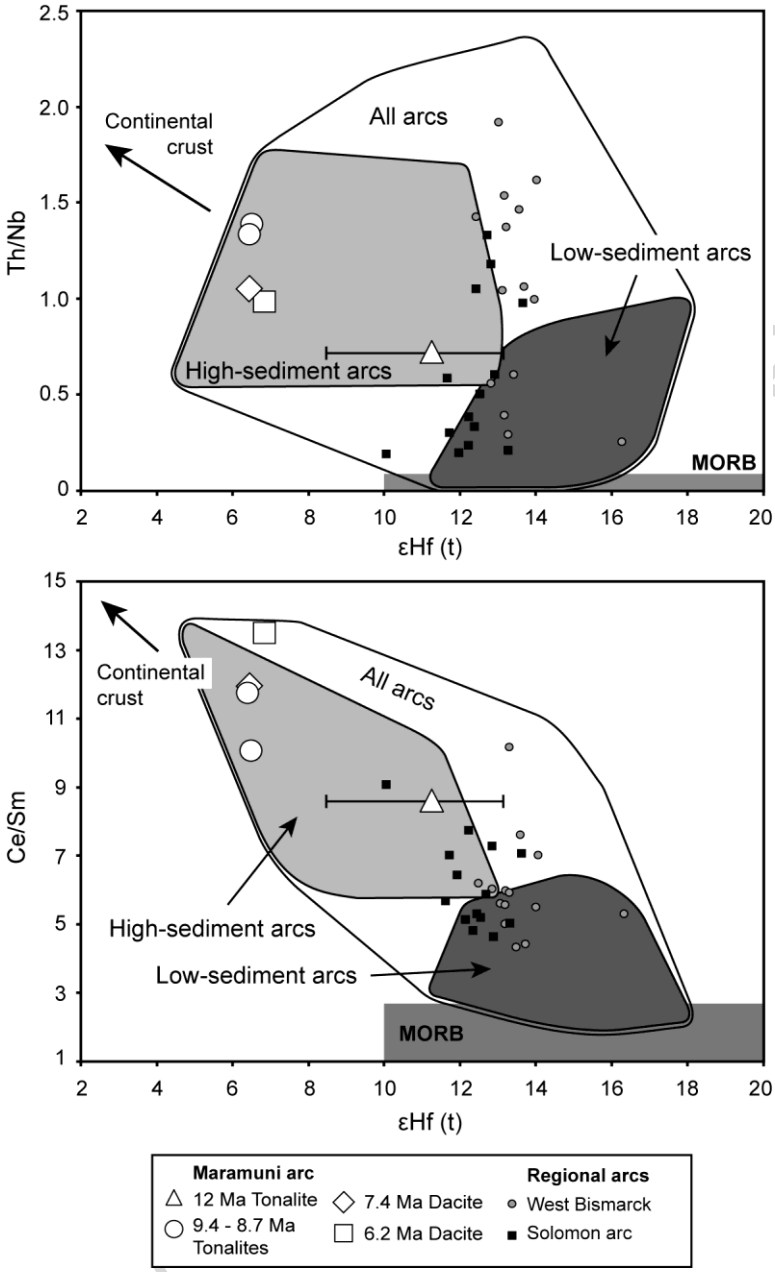

Figure 9

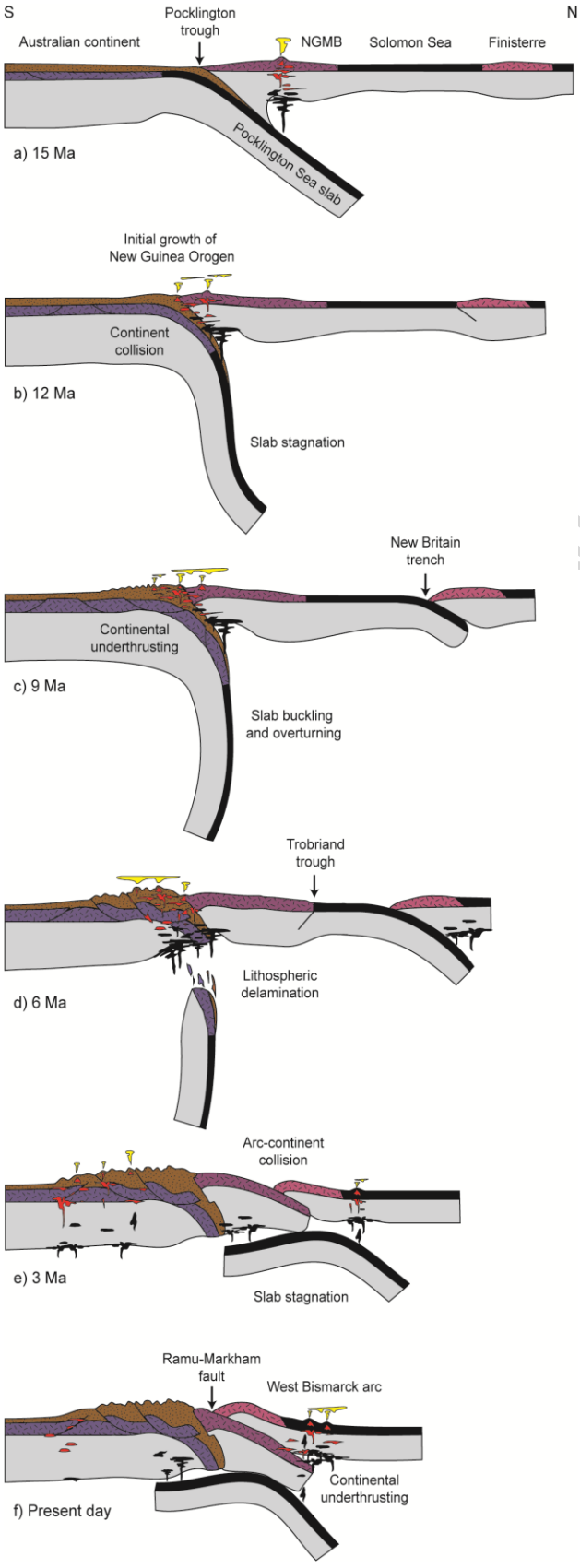

Figure 10

Table 1. Sample descriptions

Sample	Location (a) (b)	Texture	Phenocryts (c)	Matrix (c)	Alteration (c) (d)
Wamum Tonalite					
BWDD4 482	DDH 482.5–485 m	Foliated Porphyritic Medium-grained matrix	Pl	Qz Bt Mag Ap Ep	Fresh
BWDD4 585	DDH 585–588 m	Foliated Porphyritic Medium-grained matrix	Pl	Qz Bt Mag Ap Ep	Weak Ser Chl
Kokofimpa, Kainantu Tonalite					
BKDD22 468	DDH 468.2–469.5 m	Porphyritic Medium-grained matrix	Pl	Qz Pl Bt Mag Ap Zrn	Strong Ser Chl
BKDD22 472	DDH 472.7–473.9 m	Porphyritic Medium-grained matrix	Pl	Qz Pl Bt Mag Ap Zrn	Strong Ser Chl
BKDD22 475	DDH 475.6–476.4 m	Porphyritic Medium-grained matrix	Pl	Qz Pl Bt Mag Ap Zrn	Weak-Mod Ser Chl
BKDD22 511	DDH 511–512 m	Porphyritic Medium-grained matrix	Pl	Qz Pl Bt Mag Zrn	Mod-Strong Ser Chl
BKDD22 560	DDH 560.5–562.5 m	Porphyritic Medium-grained matrix	Pl	Qz Pl Bt Mag Zrn	Mod-Strong Ser Chl
BKDD22 658	DDH 658–659.5 m	Porphyritic Medium-grained matrix	Pl	Qz Pl Bt Mag Zrn	Mod Ser Chl
Dacite					
BKDD22 546	DDH 546.5–548.8 m	Porphyritic Fine-grained matrix	Pl Qz Bt	Qz Pl Mag Ap Zrn	Mod-Strong Ser Chl
BKDD22 582	DDH 582–584 m	Porphyritic Fine-grained matrix	Pl Qz Bt	Pl Qz Bt Mag Ap Zrn	Weak Ser Chl
KKS01	373139 E 9317942 N	Porphyritic Fine-grained matrix	Pl Qz Bt	Pl Qz Bt Mag Ap Zrn	Strong Ser Chl

a) Diamind drill hole (DDH) Collar location (UTM AGD66 Zone 55) and orientations:
BKDD22: 372931E 9317014N; azimuth (mag): 300°, inclination: -50°.
BWDD4: 420856E 9254093N; azimuth (mag): 330.6°, inclination: -63.2°.

b) Field cordinates in UTM AGD66 Zone 55.

c) Mineral codes :Ap, apatite; Bt, biotite; Chl, chlorite; Ep, Epidote; Mag, magnetite; Pl, plagioclase; Qz, quartz; Ser, sericite; Zrn, Zircon.

d) Alteration intensity; strong; Mod, moderate; weak; or fresh.

Table 2. Resolved ages from U-Pb dating of zircon.

Sample	Weighted Average (a)	95% Confidence	MSWD	Probability of Fit	Concordia Age (b)	2σ Error	MSWD	Probability of Fit
Wamum								
Tonalite								
BWDD04 482	11.87	0.09	0.81	0.69	11.88	0.13	0.85	0.63
BWDD04 585	12.07	0.10	0.84	0.64	12.08	0.13	0.82	0.66
Kokofimpa, Kainantu								
Tonalite								
BKDD22 472	9.41	0.10	0.70	0.81	9.41	0.17	0.69	0.80
BKDD22 560	8.78	0.12	0.54	0.90	8.79	0.24	0.59	0.85
BKDD22 511	8.70	0.10	0.90	0.59	8.70	0.19	0.87	0.63
Dacite								
BKDD22 546	7.38	0.09	0.68	0.76	7.38	0.18	0.82	0.61
BKDD22 582	6.28	0.05	0.61	0.79	6.28	0.10	0.93	0.49
KKS01	6.20	0.06	0.97	0.45	6.20	0.10	1.09	0.36

a) Weighted average age corrected for initial Th disequilibrium and common-Pb.
b) Concordia age corrected for initial Th disequilibrium.

Table 3. Representative major and trace element data.

	Wamum		Kokofimpa, Kainantu								
	Tonalite		Tonalite						Dacite		
Sample	BWDD04 482	BWDD04 585	BKDD22 468	BKDD22 472	BKDD22 475	BKDD22 511	BKDD22 560	BKDD22 658	BKDD22 546	BKDD22 582	KKS01
SiO_2	58.98	60.69	62.29	62.38	62.06	64.34	63.17	64.61	63.72	66.37	69.35
TiO_2	0.54	0.54	0.64	0.63	0.64	0.64	0.69	0.63	0.53	0.33	0.38
Al_2O_3	18.06	17.87	16.02	15.93	16.06	16.08	16.70	15.42	16.79	15.65	16.57
Fe_2O_3*	6.32	5.24	5.56	5.93	5.63	3.26	5.35	4.99	3.58	1.87	2.22
MnO	0.15	0.04	0.05	0.09	0.12	0.05	0.07	0.03	0.07	0.06	0.04
MgO	2.46	2.21	2.48	2.48	3.51	2.46	2.80	2.32	2.76	1.04	1.17
CaO	5.15	4.44	2.70	3.66	2.35	2.31	1.64	3.38	1.89	3.43	0.37
Na_2O	3.64	4.13	1.89	3.32	1.79	1.62	2.03	3.15	1.79	2.94	1.97
K_2O	1.25	2.09	3.09	1.17	2.18	3.10	2.80	2.31	3.30	2.83	4.77
P_2O_5	0.22	0.16	0.18	0.17	0.17	0.13	0.18	0.17	0.20	0.11	0.15
SO_3	0.04	0.06	0.12	0.06	0.14	0.13	0.07	0.01	0.31	0.05	0.01
LOI	3.38	2.07	5.01	4.18	5.20	5.21	4.60	2.67	5.18	5.32	3.01
Total	100.19	99.55	100.03	100.00	99.85	99.31	100.10	99.69	100.13	100.00	100.00
Sc	11	9.8	13	13	13	13	14	13	7.9	5.1	6.0
V	135	144	108	111	110	113	120	113	78	36	40
Cr	10	4.0	26	28	25	25	25	21	31	25	6.0
Co	35	41	32	35	33	28	23	60	23	15	13
Cu	166	1839	79	32	959	2473	345	381	292	7	26
Zn	119	35	51	65	122	31	48	40	68	43	103
Ga	18	17	15	17	17	14	17	16	16	16	17
As	4.5	1.1	1.9	0.7	3.0	0.8	0.8	1.2	3.5	1.6	2.1
Rb	29	40	121	40	93	99	86	70	127	70	157
Sr	699	714	182	408	230	164	157	455	178	587	262
Y	11	13	21	19	19	19	20	21	9.0	6.6	9.0
Zr	103	122	194	184	186	191	208	194	116	108	116
Nb	5.2	5.3	7.2	7.2	7.3	8.0	7.5	7.2	4.7	4.1	5.4
Mo	9.0	5.5	1.6	1.5	42	640	6.0	22	2.0	7.5	0.7
Cd	0.5	0.7	0.4	0.5	0.6	0.4	0.6	0.4	0.4	0.4	0.3
Sn	2.0	1.8	3.2	3.0	2.7	5.1	3.3	3.5	3.1	2.0	2.1
Sb	0.9	0.8	1.7	0.9	1.6	0.8	0.9	1.0	1.0	0.8	1.2
Cs	1.1	0.7	3.0	1.9	3.3	3.7	2.9	1.3	4.3	3.5	12
Ba	479	770	330	262	323	431	368	400	417	563	633
La	11	10	23	17	20	22	24	21	17	15	16
Ce	16	20	49	38	44	46	50	45	34	31	33
Pr	2.0	2.5	5.9	4.6	5.2	5.5	6.0	5.4	4.2	3.5	4.1
Nd	8.5	10.4	22.5	18.6	20.3	21.2	24.2	21.3	15.9	13.9	16.0
Sm	1.81	2.34	4.37	3.79	4.06	3.94	4.64	4.26	2.92	2.26	2.86
Eu	0.71	0.83	0.84	1.07	0.89	1.10	1.22	1.06	0.83	0.69	0.73
Gd	1.82	2.19	3.63	3.38	3.29	3.34	3.86	3.54	2.04	1.53	2.00
Tb	0.28	0.34	0.56	0.51	0.52	0.51	0.56	0.53	0.28	0.20	0.27
Dy	1.84	2.10	3.57	3.28	3.12	3.23	3.51	3.58	1.61	1.24	1.50
Ho	0.39	0.45	0.73	0.73	0.68	0.69	0.73	0.74	0.33	0.22	0.32
Er	1.12	1.27	2.10	1.99	1.91	1.87	2.05	1.96	0.87	0.61	0.82
Tm	0.19	0.19	0.27	0.29	0.27	0.25	0.30	0.34	0.12	0.11	0.14
Yb	1.24	1.34	2.30	2.30	2.18	2.00	2.10	2.35	0.89	0.67	0.77
Lu	0.20	0.23	0.32	0.34	0.35	0.33	0.30	0.37	0.16	0.10	0.13
Hf	2.81	3.20	5.02	4.91	4.79	5.00	5.51	5.27	3.08	2.99	3.28
Tl	0.05	0.07	0.51	0.17	0.58	0.47	0.40	0.22	0.53	0.43	1.38
Pb	4.0	4.6	4.9	12.4	26.9	15.1	6.4	11.0	30.6	15.1	8.8
Bi	0.10	0.07	0.38	0.07	0.44	0.24	0.04	0.53	0.47	0.06	0.07
Th	3.05	3.84	10.77	10.01	10.21	10.69	10.04	10.53	4.93	4.04	4.79
U	0.58	0.70	2.60	2.56	3.00	2.54	2.76	3.96	1.99	1.45	1.72

Table 4. Lu-Hf isotope data

Sample	Spot ID	U-Pb Spot Age (Ma)	± 2σ	$^{176}Hf/^{177}Hf$	± 1σ	$^{176}Lu/^{177}Hf$	± 1σ	εHf (t = age)	± 1σ
Wamum									
Tonalite									
BWDD4 585	2	11.9	0.4	0.283119	0.000015	0.002566	0.000019	12.1	0.5
	4	12.3	0.4	0.283050	0.000013	0.002252	0.000013	9.6	0.5
	10	11.8	0.4	0.283141	0.000013	0.004817	0.000047	12.8	0.5
	14	11.8	0.3	0.283110	0.000015	0.005415	0.000042	11.7	0.5
	22	12.0	0.5	0.283091	0.000014	0.001235	0.000028	11.1	0.5
	24	12.3	0.4	0.283152	0.000014	0.002939	0.000083	13.2	0.5
	25	12.1	0.5	0.283091	0.000014	0.001235	0.000028	11.1	0.5
	26	11.9	0.5	0.283014	0.000010	0.001510	0.000018	8.4	0.4
	27	11.9	0.5	0.283102	0.000012	0.001327	0.000022	11.5	0.4
Kokofimpa, Kainantu									
Tonalite									
BKDD22 472	4	9.1	0.5	0.282970	0.000011	0.000573	0.000011	6.7	0.4
	6	9.5	0.3	0.282984	0.000010	0.000976	0.000007	7.2	0.4
	8	9.0	0.4	0.282969	0.000009	0.000625	0.000003	6.7	0.3
	11	9.5	0.4	0.282962	0.000011	0.000510	0.000000	6.5	0.4
	15	9.3	0.5	0.282947	0.000011	0.000522	0.000002	5.9	0.4
	16	9.3	0.4	0.282963	0.000012	0.000821	0.000014	6.5	0.4
	17	9.4	0.4	0.282970	0.000014	0.000525	0.000002	6.7	0.5
	19	9.4	0.4	0.282966	0.000013	0.000866	0.000002	6.6	0.5
	21	9.5	0.5	0.282968	0.000010	0.000631	0.000005	6.7	0.4
	22	9.1	0.4	0.282936	0.000010	0.000598	0.000011	5.6	0.3
BKDD22 511	1	8.7	0.4	0.282953	0.000010	0.000926	0.000007	6.1	0.4
	7	8.9	0.5	0.282950	0.000009	0.000645	0.000003	6.0	0.3
	8	9.1	0.5	0.282965	0.000009	0.000511	0.000002	6.5	0.3
	9	8.4	0.5	0.282964	0.000009	0.000613	0.000010	6.5	0.3
	11	8.4	0.5	0.282978	0.000011	0.000716	0.000006	7.0	0.4
	16	8.9	0.5	0.282972	0.000008	0.000699	0.000009	6.8	0.3
	17	8.5	0.5	0.282960	0.000008	0.000444	0.000004	6.4	0.3
	20	8.4	0.5	0.282956	0.000010	0.000489	0.000004	6.2	0.4
	22	9.0	0.5	0.282954	0.000009	0.000612	0.000006	6.2	0.3
Dacite									
BKDD22 546	1	7.1	0.4	0.282973	0.000008	0.000990	0.000016	6.8	0.3
	3	7.4	0.3	0.282952	0.000009	0.001049	0.000006	6.1	0.3
	4	7.3	0.3	0.282964	0.000009	0.000818	0.000006	6.5	0.3
	10	7.3	0.3	0.282974	0.000016	0.001181	0.000023	6.8	0.6
	12	7.9	0.3	0.282958	0.000009	0.000915	0.000010	6.3	0.3
	14	7.8	0.3	0.282958	0.000009	0.001062	0.000006	6.3	0.3
	15	7.9	0.3	0.282958	0.000009	0.000931	0.000007	6.3	0.3
	28	7.6	0.3	0.282955	0.000011	0.000857	0.000009	6.2	0.4
	30	7.5	0.4	0.282976	0.000009	0.000746	0.000009	6.9	0.3
BKDD22 582	1	6.1	0.3	0.282981	0.000009	0.000812	0.000011	7.1	0.3
	5	6.3	0.1	0.282979	0.000010	0.000826	0.000013	7.0	0.4
	6	6.3	0.2	0.282990	0.000010	0.000825	0.000003	7.4	0.4
	7	6.5	0.2	0.282983	0.000009	0.000559	0.000004	7.1	0.3
	10	6.3	0.2	0.282969	0.000010	0.000968	0.000029	6.6	0.4
	15	6.3	0.1	0.282973	0.000009	0.001090	0.000003	6.8	0.3
	16	6.6	0.2	0.282964	0.000010	0.000739	0.000015	6.5	0.4
	17	6.3	0.1	0.282955	0.000012	0.001307	0.000011	6.1	0.4
	21	6.2	0.2	0.282975	0.000010	0.000936	0.000004	6.8	0.4
	22	6.2	0.1	0.282973	0.000011	0.001114	0.000004	6.8	0.4

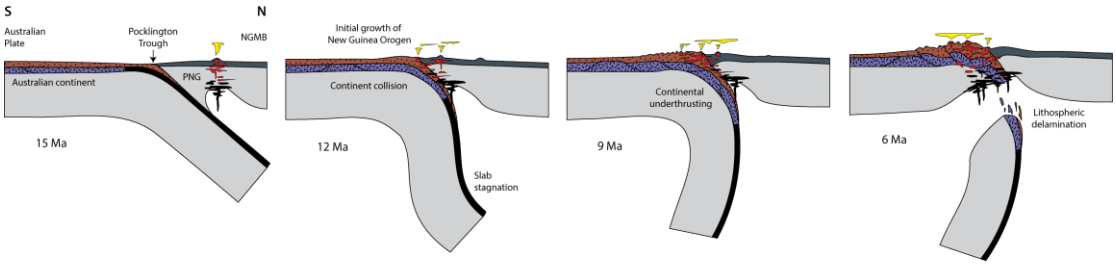

Graphical abstract

Continental collision, orogenesis and arc magmatism of the Miocene Maramuni arc, Papua New Guinea.

Robert J. Holm, Carl Spandler, Simon W. Richards

Highlights

- We present the first detailed U-Pb, Hf and geochemical study of the Maramuni arc
- A change in arc behavior correlates with Australian continent collision with PNG
- We present a new model for the Late Miocene tectonic evolution of PNG